12 The Mantle Section of Neoproterozoic Ophiolites from the Pan-African Belt, Eastern Desert, Egypt: Tectonomagmatic Evolution, Metamorphism, and Mineralization

Hisham A. Gahlan, Mokhles K. Azer, Paul D. Asimow, and Zakaria Hamimi

Abstract

The Eastern Desert (ED) Neoproterozoic ophiolites are tectonically important elements of the Arabian–Nubian Shield. Although affected by various degrees of dismemberment, metamorphism, and alteration, almost all of the diagnostic Penrose-type ophiolite components can be found, namely, lower units of serpentinized peridotite tectonite and cumulate ultramafics and upper units of layered and isotropic gabbros, plagiogranites, sheeted dykes and pillow lavas. The contacts between the lower unit (mantle section) and the upper unit (crustal section) were originally magmatic, but in all cases are now disrupted by tectonism. The mantle sections of the ED ophiolites are exposed as folded thrust sheets bearing important and distinctive lithologies of serpentinized peridotites of harzburgite and dunite protoliths with occasional podiform chromitites. The ED ophiolites show a spatial and temporal association with suture zones that indicate fossil subduction zone locations. Multiple episodes of regional metamorphism mostly reached greenschist facies with less common amphibolite facies localities. CO_2-metasomatism resulted in the development of talc–carbonate, listvenite, magnesite, and other carbonate-bearing meta-ultramafic rocks. Geochemical data from the ED serpentinites, despite some confounding effects of hydration and alteration, resemble modern oceanic peridotites. The ED serpentinites show high LOI (≤ 20 wt%); Mg# mostly higher than 0.89; enrichment of Ni, Cr, and Co; depletion of Al_2O_3 and CaO; and nearly flat, depleted, and unfractionated chondrite-normalized REE patterns. The modal abundance of clinopyroxene is very low if it is present at all. Chromian spinel survived metamorphism and is widely used as the most reliable petrogenetic and geotectonic indicator in the ED ophiolite mantle sections. The high-Cr# (mostly ~ 0.7) and low-TiO_2 (mostly $\leq$ 0.1 wt%) characters of chromian spinel indicate a high degree of partial melt extraction ($\geq 30\%$), which is commonly associated with fore-arc settings and equilibration with boninite-like or high-Mg tholeiite melts. Based on the general petrological characteristics, the ED ophiolitic chromitites are largely similar to Phanerozoic examples that have been attributed to melt–peridotite interaction and subsequent melt mixing in fore-arc settings. The comparison between the ED Neoproterozoic mantle peridotites and Phanerozoic equivalents indicates considerable similarity in tectonomagmatic processes and does not support any major changes in the geothermal regime of subduction zones on Earth since the Neoproterozoic era. The mantle sections of ED ophiolites are worthy targets for mining and exploration, hosting a variety of ores (chromite, gold, and iron/nickel laterites) and industrial minerals (talc, asbestos, and serpentine).

H. A. Gahlan
Department of Geology and Geophysics, King Saud University, Riyadh, 11451, Saudi Arabia

Geology Department, Assiut University, Assiut, 71516, Egypt

M. K. Azer (✉)
Geological Sciences Department, National Research Centre, Cairo, Egypt
e-mail: mokhles72@yahoo.com

P. D. Asimow
Division of Geological & Planetary Sciences, California Institute of Technology, Pasadena, CA 91125, USA

Z. Hamimi
Department of Geology, Benha University, Benha, 13518, Egypt

12.1 Introduction

Earth's mantle is believed to consist of a heterogeneous assortment of ultramafic rocks, ranging in composition from fertile lherzolite to depleted harzburgite and ultimately, in some circumstances, to dunite (e.g., Furnes et al. 2014).

Z. Hamimi et al. (eds.), *The Geology of the Egyptian Nubian Shield*, Regional Geology Reviews,
https://doi.org/10.1007/978-3-030-49771-2_12

Primitive, fertile mantle lithologies become depleted as a result of partial melting events in a variety of magmatic environments such as mid-ocean ridges and volcanic island arcs. The magmas resulting from such melting events are extracted and leave behind residual or depleted mantle lithologies (e.g., Jaques and Green 1980; Takahashi and Kushiro 1983; Winter 2001). Successive episodes of partial melting or reactions between peridotite and migrating melts can further deplete the residual mantle and alter the composition to highly depleted harzburgite or dunite. Note that dunite, though difficult to reach by simple melt extraction (Moores and Vine 1971), can be formed as a cumulate (e.g., Malpas 1978) or by replacive mechanisms (e.g., Quick 1981; Kelemen 1990; Kelemen et al. 1995; Allan and Dick 1996; Arai and Matsukage 1996). Areas where asthenospheric mantle reaches the lowest depths (and pressures), as well as areas affected by the addition of volatile components such as H_2O are expected to experience the largest degrees of partial melting (e.g., Kushiro 1969; Jaques and Green 1980) and so are favorable sites formation of dunite and chromitite (e.g., Quick 1981; Arai and Yurimoto 1995; Kelemen et al. 1995).

Mantle rocks can be studied in four main types of locality. Alpine-type or massif peridotites are found along continental margins and island arcs and in ancient orogenic belts as rootless lenticular bodies of serpentinized peridotite of various shapes and sizes (e.g., Coleman 1971; Jackson and Thayer 1972; Dick 1977; Sinton 1977; Arai 1980; Dilek and Newcomb 2003; and others). The Alpine-type massifs, with their extensive outcrop areas and often good exposure, provide valuable information about field relations between different mantle lithologies and give an estimate of the relative proportions of peridotitic rock species in the mantle. However, they have often experienced extensive lithospheric and surface processes that may obscure features of their original mantle history. Mantle xenoliths, by contrast, are often very fresh and directly sampled from depth. But they provide only isolated "snapshots" of a single vertical section beneath their eruption locality. Abyssal peridotites dredged directly from the seafloor, often in fracture zones along mid-ocean ridges, can be directly associated with particular mid-ocean ridge settings but are often highly altered. Intact ophiolites represent a fourth type of peridotite exposure. They have a well-known sequence of petrologic types with distinctive and easily recognizable mantle sections. When extensive tectonic dismemberment has removed them from their overlying crustal sections, as in most of the abundant examples in the Arabian–Nubian Shield (ANS), their outcrop patterns resemble those of Alpine-type peridotites. However, their characteristics allow in most cases confident assignment as the basal parts of incomplete ophiolite sequences. Each of these types of peridotite exposure can provide critical information about geochemical processes in the shallow mantle. Such processes include melt extraction, melt-rock reaction, and interaction with subduction-related fluids (e.g., Downes et al. 2001).

Study of mantle peridotites whose geodynamic and paleotectonic history are known has allowed the identification of diagnostic petrological characteristics that can, in turn, be used (with due caution) to infer the setting of ancient peridotites displaced from the context of their formation (e.g., Dick and Bullen 1984; Arai 1994a; Zhou et al. 1996; Ahmed 2013; Gahlan et al. 2015a; Gamal El Dien et al. 2016; and others). However, a range of different tectonomagmatic hypotheses have been proposed for the origin of the ED ophiolitic peridotites including (i) mid-ocean ridge (MOR) (e.g., Zimmer et al. 1995; Khalil 2007); (ii) back-arc basin (e.g., Ahmed et al. 2001; Farahat et al. 2004; Abd El-Rahman et al. 2009a; Farahat 2010); (iii) transitional back-arc basin-MORB (e.g., Abdel-Karim et al. 1996); and (iv) fore-arc (e.g., Azer and Stern 2007; Abd El-Rahman et al. 2009b; Ahmed 2013; Azer et al. 2013, 2019; Gahlan et al. 2015b).

Almost all the primary mantle minerals of the ED ophiolitic peridotites have been replaced during serpentinization or metamorphosis, except for relics of spinel and rarely of pyroxene or olivine. Hence, much of the reasoning leading to the assignment of tectonomagmatic settings for these rocks has been based on the chemistry of intact primary spinel (e.g., Dick and Bullen 1984; Arai 1992 1994a; Zhou et al. 1996). Depleted mantle residual to high degrees of partial melt extraction is most often found in the fore-arc of subduction zones and characterized by Cr-rich spinel (Cr# = molar Cr/[Cr + Al] > 0.6). On the other hand, MOR settings unrelated to subduction zones typically leave more fertile residues that have experienced lower degrees of partial melt extraction and contain more Al-rich spinel (Cr# < 0.6) (e.g., Dick and Bullen 1984; Arai 1994b; Zhou et al. 1996).

More information on the Neoproterozoic-age ophiolitic mantle peridotites is needed, particularly since the suggestion of Wynne-Edwards (1976) that there have been important changes in Earth's geothermal regime since the upper Proterozoic. If issues related to severe serpentinization and metamorphism can be overcome, the mantle sections of the Neoproterozoic ophiolites of the Egyptian Eastern Desert (ED) are of great scientific interest for understanding such general questions of the geodynamic evolution of the mantle as well as, more locally, the tectonomagmatic processes beneath the ANS and along the Pan-African Belt during the Neoproterozoic era (e.g., Ahmed 2013; Gahlan et al. 2015b; Gamal El Dien et al. 2016; among others).

This contribution is an overview of the geology of the Neoproterozoic ophiolitic mantle peridotites exposed in the ED of Egypt. Field relations, petrography, mineral chemistry, and whole-rock geochemistry are integrated to define

their general petrological characteristics and hence to constrain the geodynamic settings of the ophiolites. To examine the change in the geothermal regime, if any, from the Neoproterozoic to Phanerozoic era, we compare the Neoproterozoic ophiolitic peridotites of the ED to their Phanerozoic equivalents. Furthermore, given the striking metamorphism, alteration, and mineralization associated with the ED ophiolitic peridotites, we offer a discussion of types and grades of alteration and metamorphism on display and summarize their associated economic potential.

12.2 Geological Outline

The ANS is part of the East African Orogen, whose complex history includes records of the break-up of Rodinia at circa 900–800 Ma; and the evolution of numerous arc systems, oceanic plateaux, oceanic crust and sedimentary basins (e.g., Stern 1994; Stein and Goldstein 1996; Kusky et al. 2003; Kusky 2004); and obduction along convergent plate boundaries during the Pan-African orogeny (~750–650 Ma) (Stern 1994; Ali et al. 2010). The ANS in particular was assembled during the Neoproterozoic closure of the ~870–690 Ma Mozambique Ocean, and hence hosts a number of ophiolite-decorated sutures. In fact, the ANS may have the highest density of ophiolites of any Proterozoic terrane on Earth (e.g., Kusky et al. 2003; Kusky 2004; Stern et al. 2004). The occurrence of ophiolites decorating suture zones and their association with calc-alkaline rocks of island-arc affinity led several authors to frame their models of the Pan-African belts of the ANS in an Upper Proterozoic plate-tectonic context (e.g., Bakor et al. 1976; Garson and Shalaby 1976; Greenwoods et al. 1976, 1977, 1981; Shackleton et al. 1980).

Precambrian basement is exposed over an area of ~100,000 km^2 in the Red Sea Hills of the ED of Egypt (Fig. 12.1), and in the south Sinai Peninsula. Of this part of the ANS, the northern half of the East African Orogen, about 5.3% of the outcrop area is estimated to be ultramafic bodies (Dixon 1979; El Gaby et al. 1990; Hassan and Hashad 1990). The basement of the ED is comprised of four main tectonostratigraphic units. From bottom to top, these are (i) basal gneisses and migmatites, (ii) arc-type volcanic, volcano-sedimentary, plutonic, and ophiolite assemblages, (iii) the Ediacaran Hammamat and Dokhan supracrustal sequences, and (iv) syn- to late-tectonic granitoids that intrude all units (e.g., Ali et al. 2012; Hamimi et al. 2019). The ophiolites of the second main unit span an age range of about 200 Ma of ocean-floor magmatism (from 890 to 690 Ma) and up to 100 Ma (from 780 to 680 Ma) of terrane convergence and suturing (e.g., Stern et al. 2004; Ali et al. 2010). Some particular well-dated cases in Egypt, however, are concentrated in age span from ~730–750 Ma: the Gerf ophiolite at 741 ± 21 Ma (Kröner et al. 1992, Zimmer et al. 1995), the Ghadir ophiolite at 746 ± 19 Ma (Kröner et al. 1992), the Fawakhir ophiolite at 736.5 ± 1.5 Ma (Andersen et al. 2009), and the Allaqi ophiolite at ~730 Ma (Ali et al. 2010).

The tectonostratigraphic column of the Egyptian ophiolites can, if assembled, display the complete sequence of the Penrose Conference ophiolite model (Anonymous 1972), from mantle section upward to the overlying mafic plutonic sequence and then mafic volcanic rocks (Fig. 12.2). However, all ophiolites of the Egyptian ED have been variably dismembered by later tectonism. The isolated serpentinite masses in the ED were first defined as ophiolites by Rittmann (1958), although the term ophiolite in the sense of the contemporary definition was first applied to the ED cases by Bakor et al. (1976), Garson and Shalaby (1976), and Neary et al. (1976). Based on the field experiences of the authors, personal communications with other Egyptian geologists, and the published record, we have compiled a list of the best preserved and most complete ophiolites of the ED in Table 12.1.

Let us consider the mantle section of the Gerf ophiolite as a typical example of the appearance of these bodies. The mantle section is exposed in massive ridges and sheet-like bodies of serpentinized harzburgite, dunite, and rarely lherzolite. It is fault-bounded and well preserved in the troughs of major synforms (Fig. 12.3). The contact against country rocks is structural, defined by thrust faults verging to the W and SW (Fig. 12.4), suggesting orogenic stresses acting generally from the E and NE during the collision of East and West Gondwana (e.g., Kröner et al. 1987; Stern et al. 1990; Shackleton 1994; Nasr et al. 1996; Abdelsalam et al. 2003; Abd El-Rahman et al. 2009a; and references therein). Any metamorphic sole that may have developed during obduction has been concealed by the overthrust mantle section, and no contact metamorphism is observed toward the footwall. The mantle section, in places, was affected by the intrusion of syn- to late-orogenic calc-alkaline granite plutons, with narrow thermal contact metamorphic aureoles at their contacts (e.g., Khalil and Azer 2007; Gahlan and Arai 2009; Ahmed et al. 2012a).

Serpentinized harzburgite, the dominant mantle lithology, forms a screen that incorporates less abundant serpentinized dunite veins, layers, and lenses. Tectonic fabrics, foliations, and lineations are observed in the serpentinized harzburgite (Fig. 12.3). Toward the basal thrust and along faults and shear zones, the serpentinized peridotites are transformed into schistose serpentinites and talc–carbonates. The latter can be seen from a far distance as creamy-colored streaks cutting across the massive serpentinites. Concordant to sub-concordant small-scale chromitite pods, often observed in the uppermost parts of mantle sections (e.g., Ahmed et al. 2001; Gahlan et al. 2015b), are here enveloped by dunite that is, in turn, enclosed in the harzburgite screen (Fig. 12.2).

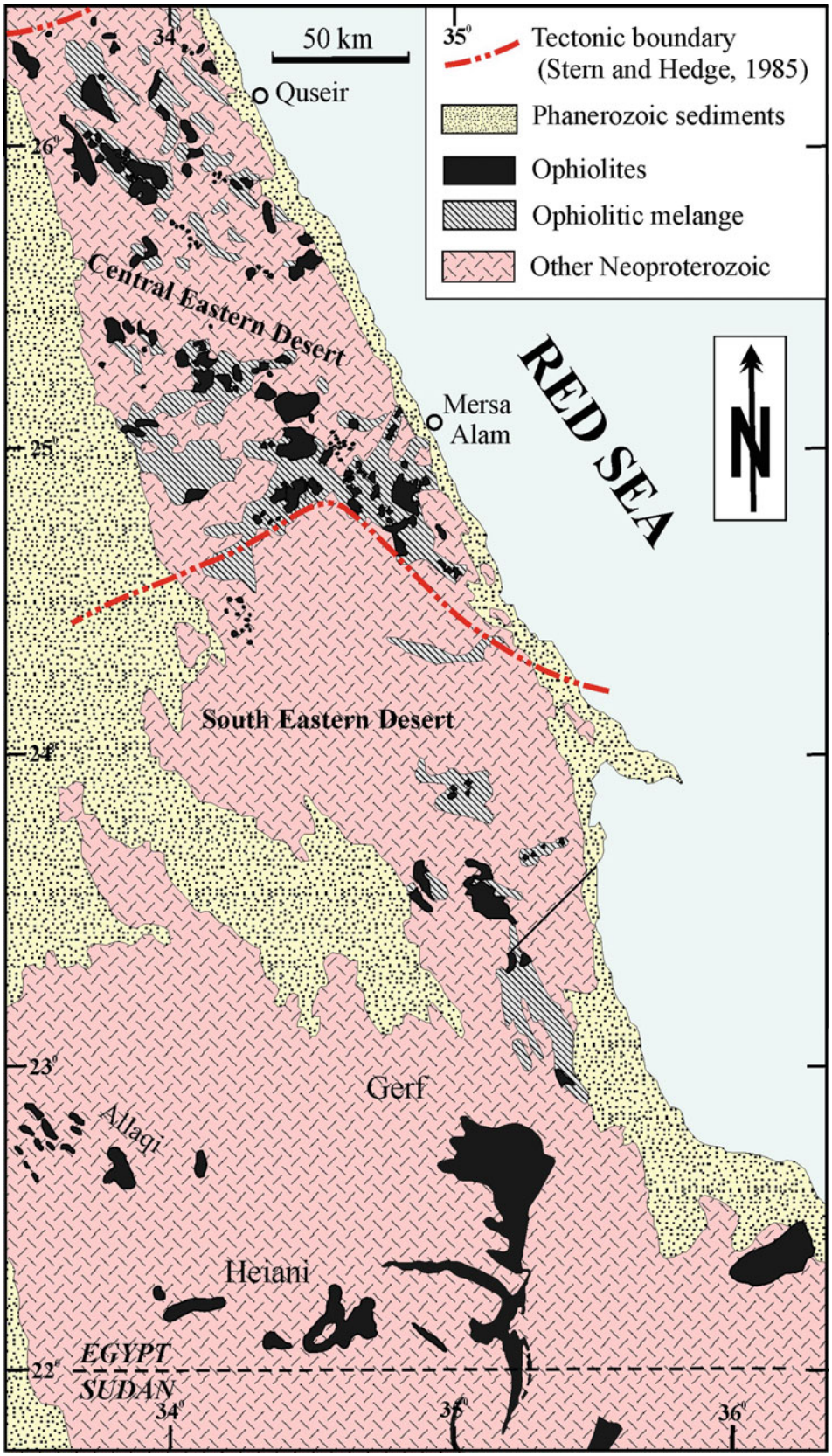

Fig. 12.1 Regional geological map showing the distribution of late Neoproterozoic ophiolitic rocks in the central and south Eastern Desert of Egypt (modified after Shackleton 1994)

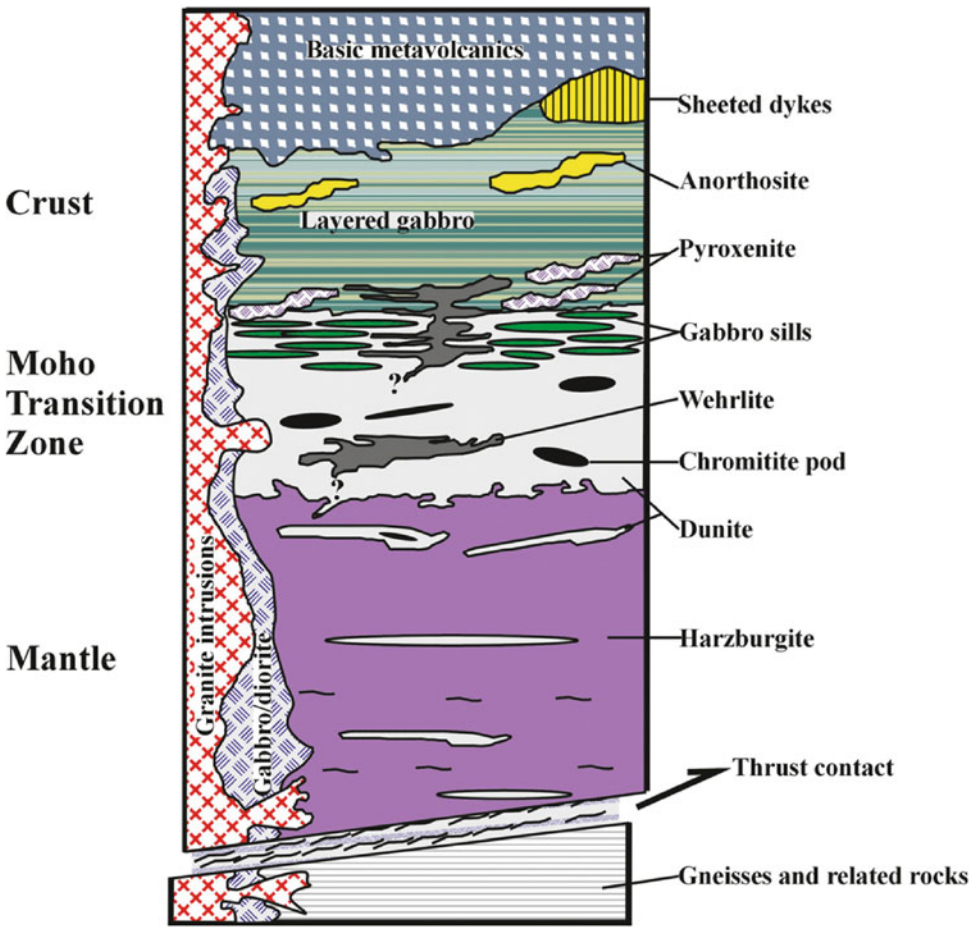

Fig. 12.2 Schematic tectonostratigraphic column of the Egyptian ophiolites (adapted from Gahlan et al. 2015b)

Table 12.1 The best preserved Pan-African ophiolites in the Eastern Desert of Egypt

Ophiolite Name	Country	References
Sol-Hamed	Egypt	Nasr and Beniamin (2001), Gahlan (2003)
Gerf	Egypt	Zimmer et al. (1995), Nasr et al. (1996), Gahlan (2003)
Wadi Ghadir	Egypt	El-Sharkawi and El-Bayoumi (1979), El-Bayoumi (1983), Khudeir (1983)
Fawakhir	Egypt	Nassief et al. (1980), El-Sayed et al. (1999)
Abu Dahr	Egypt	Gahlan et al. (2015a)

[a]The table is modified after Stern et al. (2004) and the references are cited therein

Large masses of serpentinized dunite, concordantly interlayered with serpentinized ultramafic cumulates (wehrlite and pyroxenite) and gabbro sills often define the uppermost part of ophiolite mantle sections (e.g., Ras Salatit ophiolite, Gahlan et al. 2012). This interval is called the Moho Transition Zone (MTZ) (Fig. 12.2). An interval of closely spaced gabbro sills often marks the uppermost part of the MTZ and may grade into the plutonic crustal section (Fig. 12.2). In the Gerf exposure, this initially magmatic contact between lower and upper units is now a structural contact due to severe tectonic disruption (Fig. 12.4).

Alteration of ophiolitic ultramafic rocks in the ED has led to the development of talc–carbonate, listvenite, magnesite, and (less commonly) rodingite. Talc–carbonate rocks are found both in the volcanic and mantle sections of ED ophiolites and so are divided metavolcanic-derived talc–carbonate and ultramafic-derived talc–carbonate. The majority of talc occurrences in Egypt are ultramafic-derived and may be found as separate bodies or associated with serpentinites. These rocks are characterized by their conspicuous buff/creamy color and cavernous nature. The cavernous appearance (Fig. 12.5) and porosity have been attributed to dissolution of the carbonate at or near the exposure surface by carbonic acid in meteoric water. They are generally rather uniform in mineralogical composition but vary appreciably in fabric, including massive, schistose,

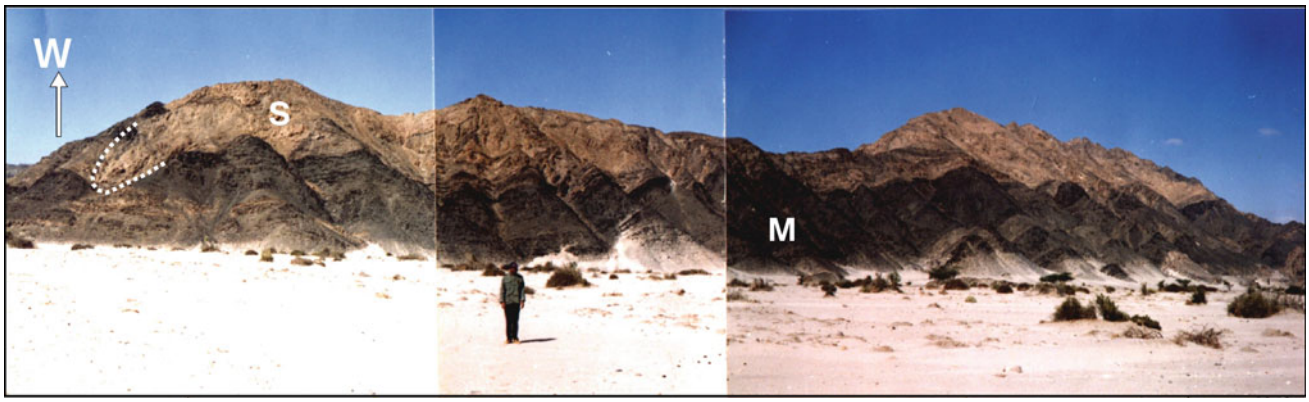

Fig. 12.3 Mosaic of field photos demonstrating massive serpentinites being preserved within the trough of a major synform at Wadi Hasium in the Gerf ophiolite nappe. Note that the original thrust contact between the low-grade metasediments (M) and the structurally overlying Gerf serpentinites (S) is folded and the eastern limb dips toward the west by 70° (270/70°) (adapted from Gahlan 2006)

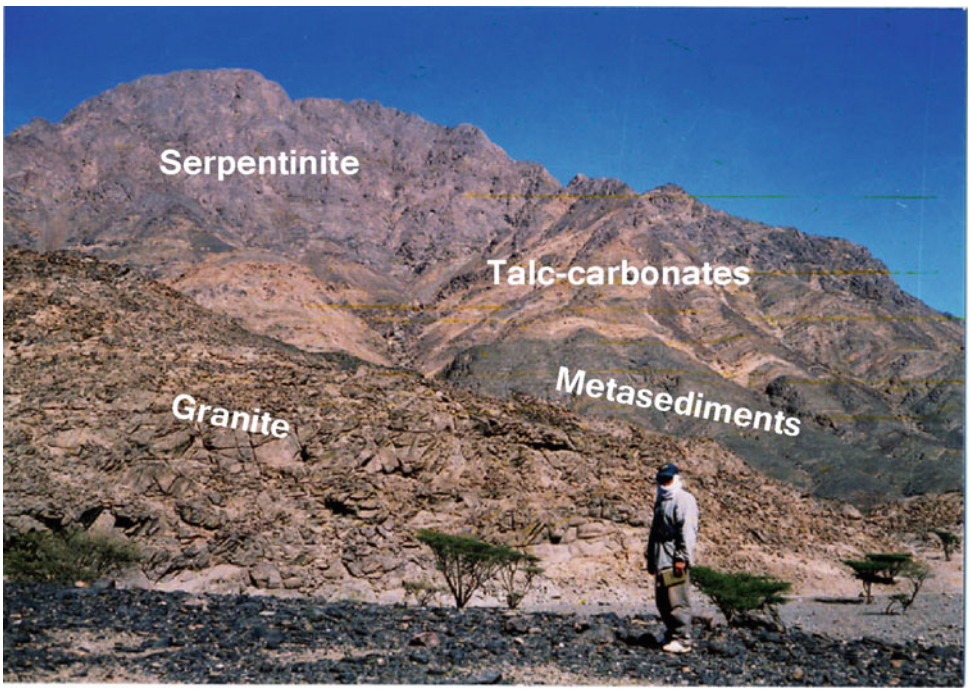

Fig. 12.4 The Gerf serpentinites thrust over low-grade metasediments, both intruded by the Shinai syn- to late-orogenic granite, with talc–carbonates demarcating the thrust contact (Wadi Shinai, Gerf ophiolite nappe; adapted from Gahlan 2006)

and gneissose varieties. The talc-rich rocks are commonly soft but they become progressively harder with increasing iron content or abundance of carbonate minerals. A few nodules and irregular pockets of magnesite and dolomite with quartz are observed in the talc-rich rocks. Some serpentinite masses are observed within the talc–carbonates (Fig. 12.6).

Listvenite bodies of various shapes and sizes are developed along shear zones. They express positive geomorphic relief relative to the surrounding rocks due to their resistance to arid-climate weathering. In poorly exposed areas, the presence of upstanding ridges of listvenite may be the only evidence for underlying altered ultramafic rocks. They mainly form dyke-like bodies or lenses hundreds to thousands of meters long (Fig. 12.7). Structural elements in the sheared listvenite rocks are generally conformable to the main plano-linear fabric of the host serpentinite. They are pink to reddish-brown in color due to iron-oxide staining. A few of the listvenite outcrops show porous textures due to supergene oxidative weathering. Locally, listvenites may be brecciated and fractured, with fractures being filled by carbonate veinlets and fine quartz ribbons.

Magnesite forms veins, stockworks, and massive bodies of snow-white color in the serpentinite country rocks (Figs. 12.8 and 12.9) and along regional faults cutting the ultramafic rocks. The boundaries of the magnesite bodies are

Fig. 12.5 Talc–carbonates at Barramiya showing their conspicuous buff/cream color and cavernous appearance

Fig. 12.6 Serpentinite mass within talc–carbonates at Barramiya

knife sharp but irregular. The magnesite veins are branched and have variable lengths and a range of widths from a few centimeters up to 1 m. Some brecciated serpentinites are present within the massive magnesite.

Rodingite appears in the ED ophiolites within serpentinized ultramafics and ophiolitic mélange, but these occurrences are only sparsely documented in the literature (Takla et al. 1992; Abdel-Karim 2000; Surour 2019). Rodingite is distinctive in outcrop; its white color with black spots rock provides a conspicuous contrast with dark-colored ultramafic host rocks. In the Gerf case, for example, rodingite appears rather homogeneous in the field, but two types of

Fig. 12.7 Listvenite dyke-like body developed along shear zones, Atud area

Fig. 12.8 Snow-white deposits of massive magnesite at Um Khariga

rodingite are recognized in ED ophiolites: Type I rodingite forms thin dykes in serpentinized peridotite (Fig. 12.10), whereas Type II rodingite forms blocks and irregular lenses in ophiolitic mélange (Azer, unpublished data). Narrow chloritite rims (blackwall) can be found between Type I rodingite and serpentinite, representing a transitional reaction zone between the two rock types. Some small serpentinized ultramafic xenoliths occur within Type II rodingite.

Fig. 12.9 Branched veins and stockwork of magnesite at Gabal Ghadir

Fig. 12.10 Rodingite dyke in serpentinized peridotites, Um Rashid area.

12.3 Structural Setting

In many areas in the ED (e.g., Beitan, Hafafit, Barramiya, El-Shalul, Meatiq, and Sibai), well-developed Pan-African thrusting can be observed separating hanging wall supracrustal unit (ophiolites and ophiolitic mélange) from infracrustal gneisses, migmatites, sheared granites, and remobilized equivalents in its footwall. Several lines of evidence support the interpretation of these contacts as thrust faults, including the contrast in metamorphic grade between supracrustal and infracrustal rocks, narrow mylonite zones, intensity of shearing and tightness of foliation, and the cataclastic nature of both litho-tectonic units close to the thrust contact. The supracrustal unit consists of dismembered blocks and masses of serpentinite, metagabbro, and metavolcanics, embedded within a matrix of low-grade metasedimentary rocks including met siltstones, slates, phyllites, and schists (Fig. 12.11). The serpentinite blocks vary in size, from small pebbles to large blocks, and may be enclosed either in a matrix of metasediments or within highly sheared serpentinite, with block boundaries usually marked by cataclasis and/or mylonitization.

Large mountainous nappes are encountered in Gerf, Muqsim, Shilman, Abu Dahr, Um Taghar, Barramiya, Shalul, and in many other areas. The Gerf ophiolitic nappe, for example, crops out immediately north of the N-to-NNE trending Hamisana Shear Zone. It is the largest nappe in the ANS, some 30–40 km in diameter, and preserves a complete N-MORB ophiolite sequence (Zimmer et al. 1995). A single zircon Pb/Pb age of 726 ± 40 Ma and a whole-rock Rb/Sr age of 551 ± 28 Ma are given by Stern et al. (1989) for a post-nappe granodioritic intrusion, whereas gabbros and basalts associated with the Gerf ophiolite give Sm/Nd whole-rock ages of 720 ± 9 Ma and 758 ± 34 Ma, respectively (Zimmer et al.,1995). Kröner et al. (1992) obtained a single zircon Pb/Pb age of 741 ± 21 Ma for layered gabbro from the Gerf ophiolite. Such ages led Zimmer et al. (1995) to conclude that the Gerf ophiolite was emplaced due to collision of island-arc complexes between 600 and 700 Ma.

The ophiolitic nappes occasionally contain variably sized blocks of amphibolite (Fig. 12.12), metagabbro, metavolcanics, and chromitite lenses. In Abu Dahr and Sefein, chromitite lenses have been systematically oriented by the effects of deformation. The ophiolitic nappes are frequently traversed by NW- (and NE-) oriented Najd-related transpressional shear zones. In many cases, shearing led to the formation of well-developed shear zone-related folds. Kinematic indicators with monoclinic symmetry and slicken lines (Fig. 12.13) reflect the overall kinematics along these Najd shears. In addition, piggyback thrusts and thrust-related structures imbricate thrust stacks (Fig. 12.14), and thrust duplexes are recorded elsewhere in the ophiolitic nappes. Thrusting propagated according to the "footwall-nucleating-footwall-vergent rule," where earlier hanging walls are carried forward in a piggyback manner, and newly formed thrusts grow in the footwalls of the older thrusts. In places, out-of-sequence thrusts are documented. Overprinting

Fig. 12.11 Close-up view showing shearing-related late chevron folding within tremolite-actinolite schist in the Hafafit Core Complex. The fold axis plunges NW (after Hamimi et al. 2018; Abo Soliman 2019)

relations demonstrate that, in most cases, thrust-related folds are older than shear zone-related folds, as documented in many deformed belts in the ED including the Mubarak–Baramiya belt, the Um Nar–Gabal Elhadid Belt, and the Wadi Khuda Belt (Hamimi et al. 2019). Thrust planes are often marked by magnesite, talc, chrysotile, and tremolite asbestos. Magnesite forms veins, stockworks, and massive bodies of snow-white color that are sometimes folded (Fig. 12.15). Far from the thrust planes, larger serpentinite blocks feature massive cores and sheared outer parts. Massive serpentinite is dark gray in color and slightly deformed. Increasing shearing intensity and tectonic transport lead to brecciated serpentinite. Highly sheared serpentinite is usually yellow to pale green. The smaller blocks and the peripheries of the large blocks show widespread shearing and milling down of the serpentinite, resulting in the formation of schistose tectonic serpentinite matrix.

In the extreme southern part of the ED, ophiolites form elongated blocks and nappes decorating the Allaqi–Heiani high-strain zone, interpreted to represent the western continuation of the conspicuous Allaqi–Onib–Sol Hamed–Yanbu arc–arc suture. The E–W extension of this ophiolite-decorated deformation suture defines the location and orientation of a fossil subduction zone between the Midyan-ED Terrane to the north and Hijaz–Gebeit–Gabgaba Terrane to the south. It is regarded by many workers (e.g., Abelsalam et al. 2003; Hamimi et al. 2019; Fowler and Hamimi 2020; Hamimi and Abd El-Wahed 2020) as a key to understanding the Neoproterozoic evolution not only of the Egyptian Nubian Shield but also the ANS as a whole.

Tectonically speaking, the rates and directions of transportation of the ophiolitic nappes have been the subject matter of detailed discussions by many workers (e.g., Greiling 1985, 1997; Abdelkhalek et al. 1992; Hamimi 1996; Abdelsalam et al. 2003; Hamimi et al. 2019; Fowler and Hamimi 2020). In these papers and references therein, one finds two proposed transport directions: W-to-WSW and N-to-NNW. The W-to-WSW transport direction is most probably a consequence of the final assembly and accretion of the whole ANS to the Saharan Metacraton (Abdelsalam et al. 2011) which was concurrent with the assembly of eastern and western Gondwana during the late Cryogenian–Ediacaran (650–542 Ma). The N-to-NNW transport direction, on the other hand, is associated with the N-directed tectonic escape of the ANS and is best preserved as N-to-NNW trending stretching lineations in ophiolitic nappes and huge blocks. The rates of transport of the ophiolitic nappes in the ED varied considerably from one deformed belt to another, depending on many parameters, including nappe size, shearing rate, and the rheology of the enclosing lithologies (Hamimi et al. 2019).

12.4 Petrography

Petrography of the ED ophiolitic mantle lithologies will be described generally in the light of their field observations. Despite extensive replacement by serpentine minerals, an experienced petrographer identifies primary mantle mineral modes with the aid of relict textures, supported by chromian

Fig. 12.12 Amphibolite block in highly sheared meta-ultramafic rocks, the northern part of Nugrus shear zone

Fig. 12.13 Slickenlines encountered along a NW-oriented shear zone, west of Meatiq dome

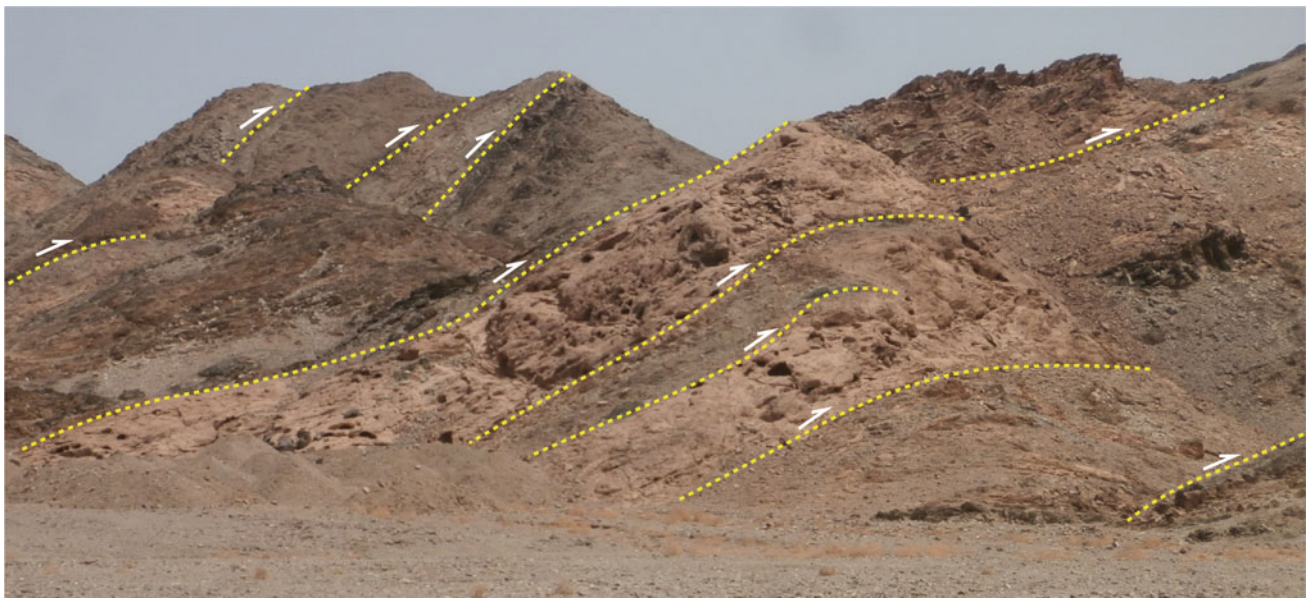

Fig. 12.14 Imbricated thrust stacks in highly sheared meta-ultramafic rocks near the Kordman Gold Mine

spinel chemistry and morphology (e.g., Arai 1980; Liipo et al. 1995; Matsumoto and Arai 2001). Harzburgite, dunitic harzburgite, and dunite are the predominant protoliths. Although serpentinization and alteration of the ED mantle peridotite rocks are pervasive, each process is variable in intensity. Considerable local differences of H_2O and CO_2-activity during metamorphism of ED mantle sections led to the development of various categories of metaperidotite, including lizardite serpentinite, carbonated metaperidotite, magnesite–antigorite serpentinite, anthophyllite-bearing serpentinite, and talc–carbonate rocks (e.g., Gahlan and Arai 2009; Ahmed et al. 2012a; Gahlan et al. 2015b among others). The term serpentinite is applied for a rock composed of $\geq 50\%$ serpentine-group minerals (e.g., Coleman 1971),

Fig. 12.15 Folded magnesite in the vicinity of Gabal Zabar

and likewise carbonate-bearing rocks as rocks containing $\geq 50\%$ carbonates. Widespread oxidative low-temperature alteration lends the pervasive reddish-creamy color to many carbonate-bearing outcrops (Fig. 12.16). Along shear zones and around igneous intrusions, the serpentinites are transformed into talc–carbonates and carbonated metamorphic peridotites, where the original textures are partly or completely obliterated by recrystallization (e.g., Gahlan and Arai 2009). Moreover, intensive shearing resulted in crudely foliated fine clastic rocks.

Lizardite serpentinites of harzburgite parentage are the most common rock type in the ED ophiolite mantle sections and represent the lowest degree of metamorphism. They are usually massive, fine-grained, and dark grayish-green in color with green patches and yellowish-green weathered surfaces (Fig. 12.17). Petrographically, they consist mainly of serpentine minerals (lizardite/chrysotile), variable amounts of carbonate minerals (magnesite and dolomite), subordinate relics of primary mantle minerals (olivine, pyroxene, and chromian spinel), and accessory sulfides and magnetite. They are dominated by pseudomorphic microtextures (e.g., O'Hanley 1996).

Generally, harzburgite protoliths had almost exclusively protogranular textures except those close to shear zones and thrust contacts. Even when completely serpentinized, it is possible to recognize pseudomorphs after primary orthopyroxene (bastite texture, Fig. 12.18a) and olivine (mesh texture, Fig. 12.18b). Bastite is typically low in modal abundance (≤ 20 vol.%); the subhedral shapes and uniform texture indicate one precursor pyroxene, probably orthopyroxene (Fig. 12.18a). Most bastites are composed of lizardite with lesser chrysotile (e.g., Whittaker and Zussman 1956; Page 1967); we have never seen antigorite bastite, despite some published descriptions (Hess et al. 1952; Wicks and Whittaker 1977). Chromian spinel forms deep reddish-brown, anhedral, and embayed crystals with submetallic luster in reflected light. Alteration products with higher reflectivity and sharp optical boundaries with unaltered parts are developed along rims and cracks of chromian spinel (Fig. 12.18c), often in order from ferritchromite through Cr–magnetite to magnetite. The degree of spinel alteration is commonly higher in serpentinized harzburgite than in dunite. Chromian spinel commonly includes Al–serpentine, chlorite, olivine, dolomite, calcite, or sulfides.

Antigorite serpentinites are generally massive and fine-grained. They occur as dark greenish-gray lenticular layers and lenses within serpentinized harzburgite. Occasionally, they are dissected by parallel sets of very small-scale oriented shear zones and fractures filled with carbonates (mostly magnesite). Petrographically, they consist mainly of antigorite with or without fresh relics of primary silicates, magnesite (rarely dolomite), and subordinate amounts of chromian spinel, magnetite, and sulfides (mainly pentlandite). Relics of primary minerals in antigorite serpentinite from the Gerf ophiolite, e.g., include dark brown patches of anhedral, cracked olivine (Fig. 12.18d), and pyroxene (Fig. 12.18e) set in a dense fine-grained groundmass of serpentine (Gahlan et al. 2015b). Antigorite flakes

Fig. 12.16 Peridotite pervasively altered to reddish-cream carbonates at Barramiya

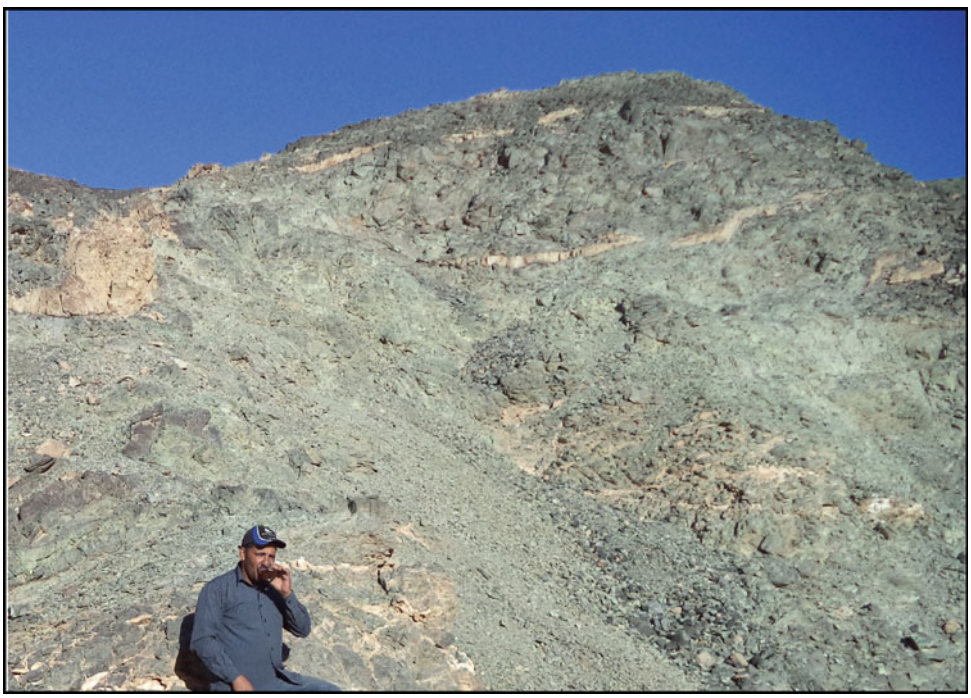

Fig. 12.17 Yellowish-green weathered surfaces of lizardite serpentinites of harzburgite parentage at Gabal Ghadir

are occasionally replaced by (or included in) carbonate minerals, principally magnesite. Larger antigorite crystals host magnetite dust or fine granules. The process of recrystallization to antigorite was accompanied by the development of non-pseudomorphic interpenetrating fabrics (e.g., O'Hanley 1996), including rosette or knitted structures, flame texture of Francis (1956), and thorn texture of Green (1961) (Fig. 12.18f). Olivine, if any, is found as relics set in a dense groundmass of antigorite. Chrysotile develops as veinlets (Fig. 12.18g) or along relict olivine fractures and cracks; the margins of chrysotile veins are embayed by antigorite. Deep reddish-brown chromian spinel forms euhedral to rounded crystals, which is a characteristic crystal form of spinel inherited from dunite protoliths (Fig. 12.18h).

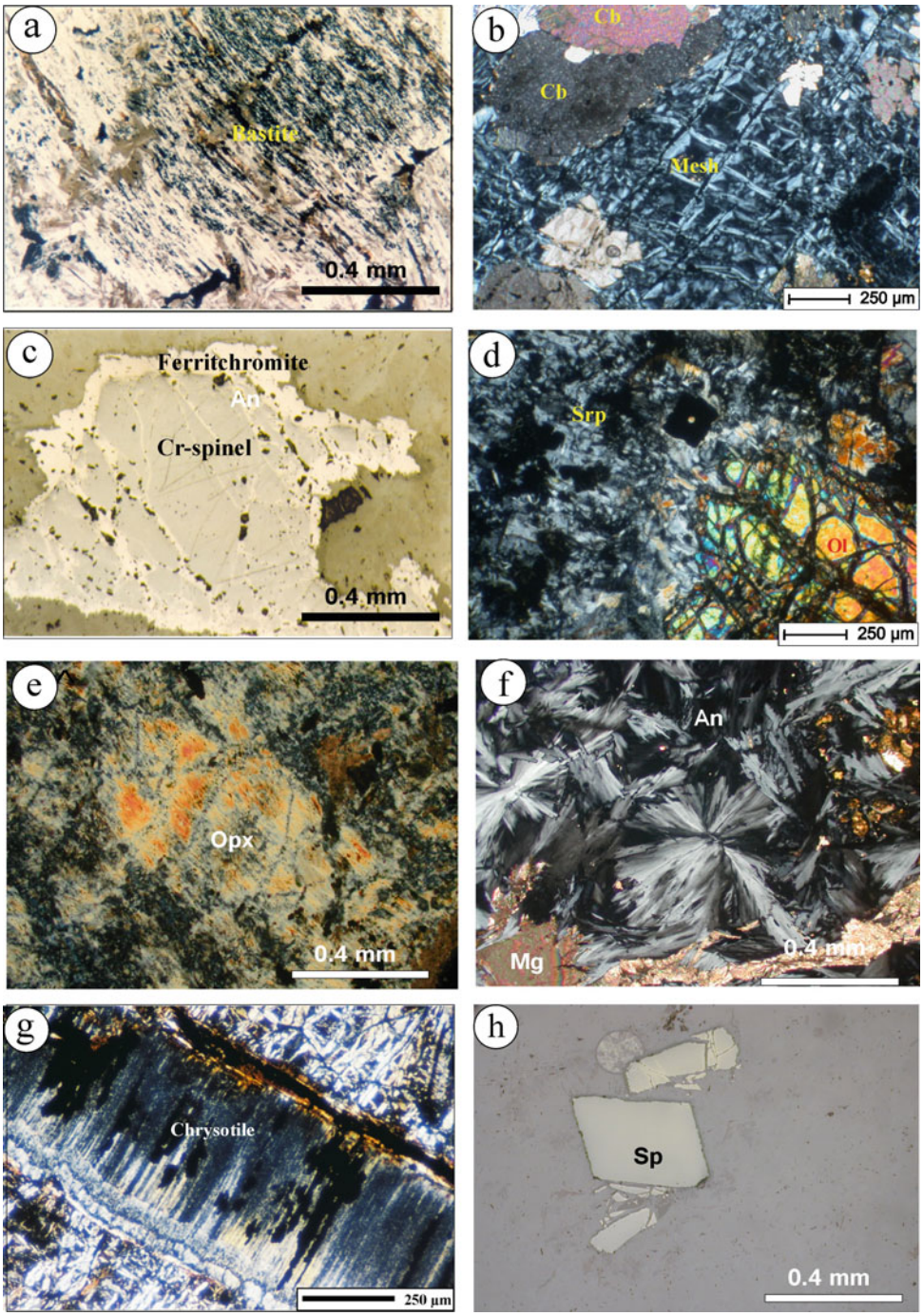

Fig. 12.18 Photomicrographs showing petrographic textures: (a) bastite texture within serpentine minerals; (b) mesh texture within serpentine minerals; (c) chromian spinel crystal altered along the margins and cracks to ferritchromite; (d) fresh relics of olivine in serpentinized dunite; (e) fresh relics of orthopyroxene in serpentinized harzburgite; (f) antigorite showing feather, rosette, and flame textures with carbonates; (g) chrysotile veinlets cutting antigorite; and (h) euhedral chromian spinel crystals in serpentinized peridotite. All images in cross-polarized transmitted light except (a) in plane-polarized transmitted light, (c) in reflected lighted, and (h) is backscatter image

The degree of spinel alteration is commonly lower than that in harzburgite. Alteration to Cr–magnetite and magnetite, with less developed ferritchromite, is found only along grain boundaries and cracks. Sulfides, chlorite, magnesite, dolomite, and Cr–tremolite are commonly included in chromian spinel. Magnetite forms anhedral equant grains, randomly distributed throughout the rocks or aligned in veinlets along cracks. Magnetite is less abundant in serpentinized dunite than in harzburgite.

Both massive and disseminated *chromitites* are found in the mantle sections of ED ophiolites. Massive chromitite (Fig. 12.19a) is composed mainly of coarse, equidimensional, euhedral to anhedral crystals of chromian spinel (>92 vol.%) with some interstitial serpentine minerals and rare olivine. Chrome spinel is commonly unaltered or may show only slight alteration to ferritchromite along grain margins and cracks. Very small olivine inclusions are observed within the chromian spinel. Cumulate, chain structures, and

banding are the most common textures of the massive chromitite, typical of magmatic crystallization (Pal and Mitra 2004). Disseminated chromitite (Fig. 12.19b) consists of chromian spinel (40–70 vol.%), intergranular serpentine minerals and rare olivine, chlorite, and opaques. Compared to the massive chromitite, most chromian spinel grains in disseminated chromitite are more euhedral, smaller, and more altered, with highly porous rims of ferritchromite. The greater intensity of alteration in disseminated chromitites can be attributed to easier subsolidus elemental redistribution with neighboring silicate phases, which are nearly absent in massive chromitite.

The ED ophiolite mantle sections also feature a number of distinctive alteration products, including talc–carbonates, listvenite, and magnesite with less common anthophyllite and rodingite rocks. Metasomatic alteration of serpentinite to *talc–carbonates* occurs to variable extents. The talc–carbonate rocks are fine-grained with brownish-yellow to reddish-brown color. They are composed essentially of talc (>75 vol.%) with subordinate serpentine, carbonate, and opaques (Fig. 12.19c). Talc occurs as fine aggregates or as platy or micaceous grains. Carbonates, principally magnesite with minor dolomite and occasional calcite, are irregularly distributed and form coarse-grained aggregates. Opaque minerals include magnetite, chromian spinel, and sulfides.

Listvenite (also spelled "listwaenite" and "listwanite") is an unusual rock type with a distinctive mineralogy of Cr-rich muscovite (fuchsite), quartz, and carbonates. It represents the end product of carbonatization, potassic alteration, and silicification (Halls and Zhao 1995; Azer 2013; Gahlan et al. 2018). Petrographically, Azer (2013) and Gahlan et al. (2018) distinguished listvenite into two types, silica-rich and carbonate-rich. The presence of fuchsite in the silica-rich variety indicates that it is typical listvenite, while the absence of fuchsite in the carbonate-rich variety suggests that "listvenite-like rock" is a more precise name for it. Most likely these two types of listvenite are formed by alteration under different conditions or in fluids of different

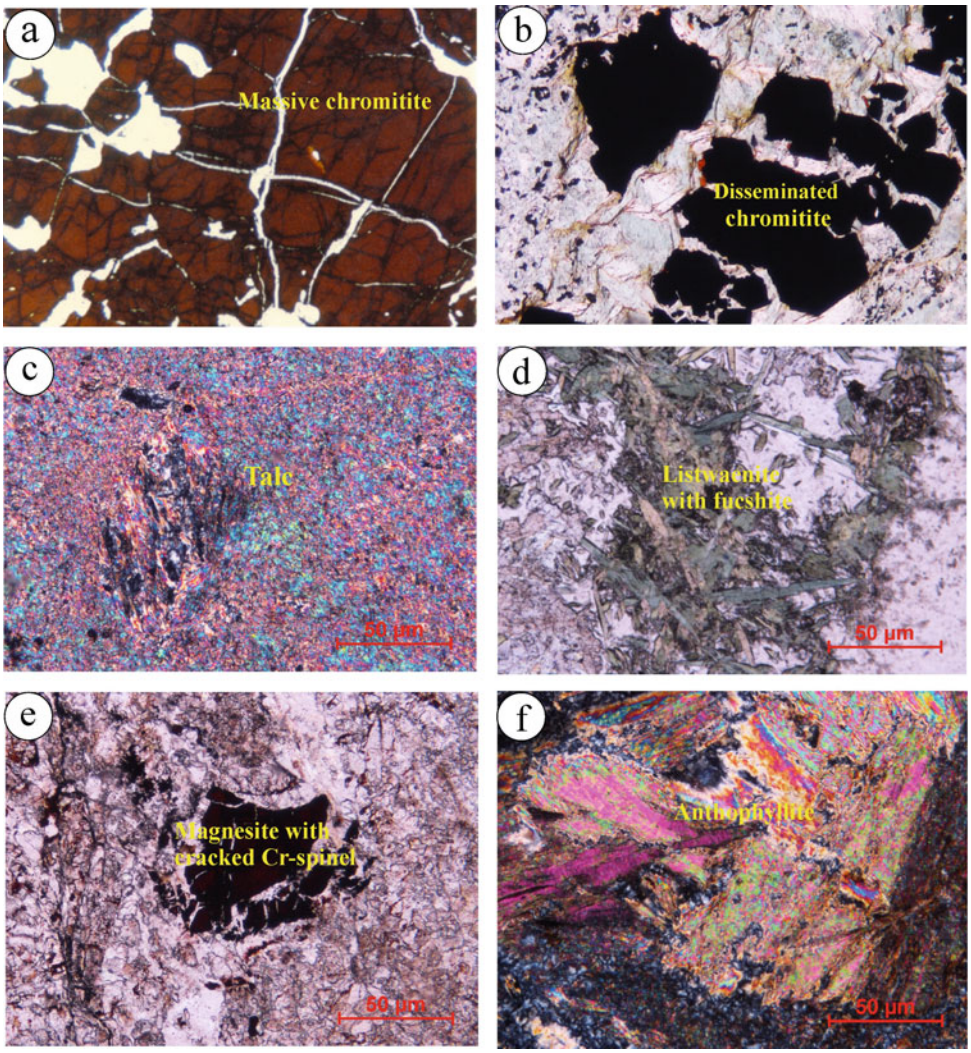

Fig. 12.19 Photomicrographs of alteration features: (a) massive chromitite with minor serpentine along grain boundaries and cracks, (b) disseminated chromitite, (c) fine aggregates of talc, (d) listvenite with fuchsite, (e) cracked chromian spinel crystals within massive magnesite, and (f) anthophyllite rock. All images in plane-polarized transmitted light except (c, f) are in cross-polarized transmitted light

compositions, rather than trapping progressive states along a single alteration path. In general, listvenites are composed of carbonates (magnesite and breunnerite with minor calcite), quartz, Fe–Ti oxides, serpentine, chromian spinel, and chlorite. The Si-rich variety also features the characteristic fuchsite as an accessory mineral in the form of flakes, fine disseminated crystals, and thin bands with a perfect cleavage in one direction (Fig. 12.19d).

Magnesite ores in the ED occur as veins and massive bodies associated with serpentinite. Vein magnesite is pure magnesite and predominantly cryptocrystalline in texture, with sharp contacts against enclosing serpentinites. Rare angular fragments of host rocks are observed near some vein margins but there are no other silicate minerals in the veins. Massive magnesite consists essentially of magnesite with minor dolomite and calcite. Rare chromian spinel crystals similar to those in the host rocks occur within the massive magnesite (Fig. 12.19e). Angular to sub-angular fragments of serpentinite and rare quartz veinlets are observed within massive magnesite pods.

Anthophyllite rock was formed due to the alteration of harzburgite through the introduction of SiO_2-rich fluids derived from the country rocks. It was formed at temperatures around 500 °C (Azer, unpublished data). Anthophyllite rock is composed mainly of fibrous anthophyllite with subordinate amphibole and opaque minerals (Fig. 12.19f).

12.5 Geochemistry

Most published chemical analyses from the mantle sections of ED ophiolites are from serpentinite samples (e.g., Zimmer et al. 1995; Abd El-Rahman et al. 2009a, b; Azer et al. 2013; Khalil et al. 2014; Obeid et al. 2016; Boskabadi et al. 2017; Abdel-Karim et al. 2018; Gahlan et al. 2018; among others). All analyzed serpentine samples contain abundant water and carbonate, with high LOI (typically greater than 10% and less than 20%). They have Mg# (100*Mg/[Mg + Fe^T] on a molar basis) greater than from 89, as do modern oceanic peridotites (Bonatti and Michael 1989). The typical Mg# values and very low K_2O and Na_2O contents indicate limited elemental mobility during serpentinization. Also, the very low concentrations of CaO in carbonate-free serpentinites are representative of metamorphic ophiolitic peridotites (Coleman 1977), as opposed to ultramafic cumulates.

Due to the extensive replacement of primary minerals by serpentine, estimates of the modal percentages of primary minerals are imprecise and classification by a modal scheme such as Streckeisen (1976) can only be approximate. Some authors have instead applied a classification using normative mineralogy based on whole-rock chemistry, neglecting any changes to anhydrous composition that may have accompanied serpentinization (e.g., Azer and Khalil 2005; Gahlan et al. 2015a; Khalil et al. 2014; Obeid et al. 2016; Azer et al. 2019). This places the majority of serpentinized ED ultramafic samples in the harzburgite and dunite fields, with rare lherzolite (Fig. 12.20a), in agreement with petrographic and field assessments.

Geochemical data indicate that addition or subtraction of elements other than water and perhaps silica was very limited for massive serpentinites (i.e., away from shear zones and faults), encouraging us to compare these compositions with those of peridotites from modern tectonic settings. The very low abundance of Al_2O_3 in the ED serpentinites (Azer and Stern 2007; Abd El-Rahman et al. 2009a, b; Gahlan et al. 2015b; Obeid et al. 2016; Abdel-Karim and El-Shafei 2018) resembles "oceanic trench" peridotites as defined by Bonatti and Michael (1989). Similarly, the low mean CaO

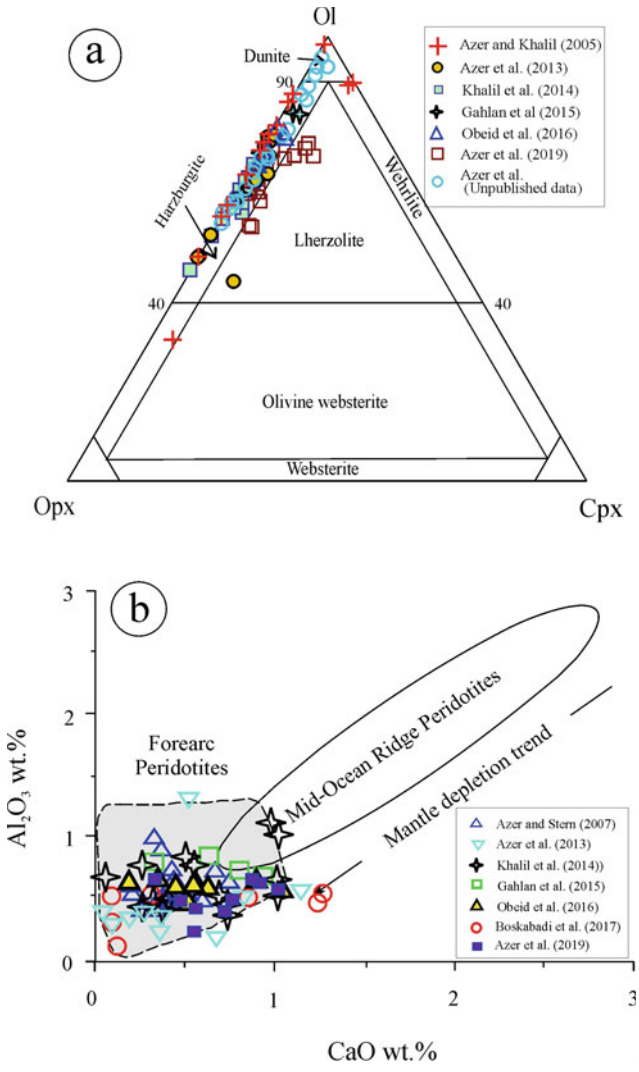

Fig. 12.20 **a** Nomenclature of ED serpentinized ultramafic rocks based on Ol–Opx–Cpx normative composition, compared to field and petrographic assignment (after Coleman 1977) and **b** Al_2O_3 versus CaO diagram for ED serpentinized ultramafic rocks compared to fields of Ishii et al. (1992)

(<1%) suggests that protoliths were poor in clinopyroxene and affinities with much depleted oceanic peridotites (Bonatti and Michael 1989). Moreover, on the Al_2O_3 versus CaO diagram, the Egyptian serpentinites plot with harzburgites recovered from modern intra-oceanic fore-arcs (Fig. 12.20b).

As expected for peridotites, the trace element contents of the Egyptian serpentinites are highly variable, but they are uniformly depleted in most trace elements with unfractionated flat REE pattern, and enriched in the compatible elements Cr, Ni, and Co.

12.6 Discussion

12.6.1 Protolith and Geodynamic Setting

The ophiolitic rocks of the ANS have long been the subject of research because they represent important elements for reconstructing the geodynamic evolution of the Pan-African belt. In the northern ANS, ophiolites on both sides of the Red Sea are generally interpreted to have formed in supra-subduction zone (SSZ) tectonic settings (e.g., Nassief et al. 1984; Pallister et al., 1989; El Sayed et al. 1999; Ahmed et al. 2001; Farahat et al. 2004; Stern et al. 2004; Azer and Stern 2007; Abd El-Rahman et al. 2009b). Seafloor spreading is necessary to form SSZ ophiolites, whether in the fore-arc during the infant arc stage of subduction initiation or in a back-arc basin (Pearce 2003; Stern 2004). Resolving which of these environments is represented by a particular SSZ ophiolite is important because fore-arc ophiolites mark the formation of new subduction zones (Stern 2004) in episodes often associated with major plate reorganizations. In contrast, back-arc basins can form at any time in the evolution of a convergent plate margin.

Most assessments of tectonic setting for ED ophiolites have focused on the trace element composition of basic rocks (lavas and gabbros) and have rarely considered the abundant mantle sections. However, interpretation of tectonic setting for Neoproterozoic ophiolitic rocks on the basis of metavolcanic and metagabbro samples encounters difficulties due to the effects of fractional crystallization and alteration. Even when these problems are minimized, it can be very difficult to distinguish the chemical compositions of fore-arc and back-arc lavas (Azer and Stern 2007). The geochemistry of lavas of the ED ophiolites appear to be transitional between island-arc basalt and MORB, which has led a number of authors to back-arc environments for Egyptian ophiolites (e.g., El Sayed et al. 1999; Farahat et al. 2004; Abd El-Rahman et al. 2009a). However, the transitional character of the ophiolitic lavas is simply due to their hydrous nature and the effects of added slab-derived components (Azer and Stern 2007), which is not restricted to the back-arc. Building of the relatively recent discovery and exploration of fore-arc spreading during subduction initiation (Shervais et al. 2004; Stern 2004), a number of recent papers have instead argued for a fore-arc setting for the Egyptian ophiolites (Azer and Stern 2007; Khalil and Azer 2007; Gahlan et al. 2015a 2018; Azer et al. 2019; among others).

Although controversy over the detailed tectonic environment of the ED ophiolites, the case for fore-arc affinity is strong. Phanerozoic boninites appear to be restricted to fore-arc settings (e.g., Murton 1989; Johnson and Fryer, 1990; Bédard 1999; Beccaluva et al. 2004). Magmas with boninitic affinities have been reported from the ANS (Wolde et al. 1993; Yibas et al. 2003; Katz et al. 2004; Teklay 2006), and in particular such affinity has been found in mafic members of some ED ophiolites (e.g., El Sayed et al. 1999; Abdel Aal et al. 2003; Saleh 2006).

In order to use evidence from the mantle sequences of the ED ophiolites to gain further insight into tectonic affinity, one must first consider possible artifacts. Serpentinization has obviously affected the ultramafic units of the ED ophiolites, but in many cases serpentinization may be an essentially isochemical process (Coleman and Keith 1971; Donaldson 1981; Shiga 1983, 1987), except for Ca and mobile incompatible trace elements have been also leached from the peridotites during serpentinization. Ni, Cr, Co, and V, in particular, are compatible and relatively "immobile" during alteration (e.g., Hébert et al. 1990; Pereira et al. 2003). In the ED cases, bulk serpentinites show uniformly high Mg# and enrichment in Ni, Cr, and Co. Together the high Cr# (up to 0.8) of the intact spinel, these features all suggest high degrees of partial melt extraction (e.g., Gülacar and Delaloye 1976; Dick and Bullen 1984; Arai 1994a; Ishiwatari et al. 2003).

The marked depletion observed in incompatible elements, as well as the nearly flat, depleted, and unfractionated REE chondrite-normalized pattern of the ED serpentinized peridotites indicates highly refractory peridotite protolith (harzburgite and dunite), high degrees of partial melting and high melt/rock ratio (e.g., Roberts 1992; Bodinier and Godard 2003; Gahlan et al. 2015b; Obeid et al. 2016; among others), though it may also reflect later modifications. Moreover, the parental melt of the ED peridotites is suggested to be little fractionated by plagioclase crystallization, which is supported by the almost nil Eu* negative anomaly (e.g., Drouin et al. 2009; Obeid et al. 2016). The behavior of fluid-mobile elements, Au, As, S, LILE, and Pb in the ED serpentinites, could be attributed to alteration and/or the action of fluids produced by dehydration of subducted slab (e.g., Gahlan et al. 2015b; Boskabadi et al. 2017).

In some places, metamorphism, alteration, and deformation have been severe enough to obliterate primary textures and mineralogy. However, in most of the massive

serpentinites, one can still identify primary mantle lithologies with the aid of relict textures (e.g., bastite and mesh serpentinite) and chromian spinel chemistry and morphology (e.g., Arai 1980; Liipo et al. 1995; Matsumoto and Arai 2001). The relict protogranular texture and vermicular shape of chromian spinel in many localities may indicate harzburgites that did not experience significant post-magmatic deformation.

Spinels are the only igneous minerals that retain most of their original chemistry in the serpentinized peridotites. Even in completely serpentinized ultramafic rocks containing no relics of primary silicate minerals, the chemical composition of unaltered accessory chromite has been widely recognized as a potentially important petrogenetic indicator (e.g., Barnes and Roeder 2001; Sobolev and Logvinova 2005; Arif and Jan 2006). Spinel from MOR and back-arc basin peridotites generally have Cr# <50 (Barnes and Roeder 2001; Ohara et al. 2002), whereas spinel in fore-arc peridotites generally has higher Cr# (up to 80) and spinel from boninites typically has Cr# of 70–90 (Ohara and Ishii 1998; Stern et al. 2004). The Cr# of spinel in ED ophiolitic peridotites is mostly >60 (e.g., Khalil and Azer 2007; Khalil et al. 2014; Gahlan et al. 2015b; Azer et al. 2019) and similar to those of modern fore-arc peridotites. The negative correlation between Cr# and Mg# of chromian spinel (Fig. 12.21a; see also Fig. 12.8 in the companion paper by Azer and Asimow in this volume) may reflect variable partition coefficients for Mg and Fe between chromian spinel and olivine or silicates (Irvine 1965; Dick and Bullen 1984).

The high Cr# of chromian spinel from the ED peridotites is combined with low TiO_2 contents, mostly <0.3 wt% (Fig. 12.21b). This feature is also consistent with high degrees of near-fractional partial melting and melt extraction (Mysen and Kushiro 1977), as expected for the mantle wedge in SSZ (fore-arc) settings (e.g., Dick and Bullen 1984; Bonatti and Michael 1989; Arai 1992, 1994a). Ohara and Ishii (1998) found similar accessory chromian spinel with high Cr#, up to 0.8, in fore-arc peridotites from the Mariana Trench. Thus, the spinel chemistry in the mantle sections Neoproterozoic ED ophiolites strongly supports the inferences previously drawn from their volcanic sections that they are fragments of oceanic lithosphere that experienced boninitic or high-Mg tholeiitic magmatism in an SSZ setting (e.g., Pearce et al. 1984; Arai 1992, 1994b).

The fresh relics of primary olivine found in most peridotites, even when strongly serpentinized, can provide further insight into the tectonic setting for the protoliths (Parkinson and Pearce 1998; Pearce et al. 2000; Coish and Gardner 2004). Relict olivine in Egyptian ED serpentinites is Mg-rich, with Fo content >88 (Khudeir 1995; Khalil and Azer 2007; Gahlan et al. 2015b; Khalil et al. 2014; Obeid et al. 2016; Gahlan et al. 2018, Azer et al. 2019), much like relict olivine analyzed in other ANS ophiolites (e.g., Ledru and Auge 1984; Nassief et al. 1984; Stern et al. 2004). In this regard, they resemble olivine in fore-arc peridotites (Arai 1994b), interpreted to be residues after extensive melt extraction. Compositions of coexisting olivine and spinel (Fig. 12.22a) in the ED ophiolitic serpentinites further supports a fore-arc setting for these ophiolites (e.g., Khalil and Azer 2007; Khalil et al. 2014; Gahlan et al. 2015b; Obeid et al. 2016; Gahlan et al. 2018, Azer et al 2019).

The low Al_2O_3 and high Mg# of fresh relics of orthopyroxene in serpentinized peridotites from the ED ophiolites are also consistent with those found in highly depleted fore-arc peridotites (e.g., Ishii et al. 1992; Bonatti et al. 1993). Finally, despite the scarcity of clinopyroxene in the highly depleted ED peridotites, exceedingly rare fresh clinopyroxene relics can be found and analyzed and, again, their compositions are characteristic for intra-oceanic fore-arc regions (Fig. 12.22b).

12.6.2 Alteration and Metamorphism

The mantle sequences of the ED ophiolites preserve evidence of a variety of post-magmatic fluid interaction processes that sample a range of temperatures, pressures, and fluid compositions. Alteration and metamorphism may have occurred at the ocean floor, below the oceanic crust, during and after tectonic emplacement, or upon recent exposure. Hence, a variety of origins and compositions have been proposed for metamorphic fluids affecting the ANS ophiolites (e.g., Azer 2013; Gahlan et al. 2018): (i) mantle-derived CO_2-bearing fluids (e.g., Boskabadi et al. 2017; Hamdy and Gamal El Dien 2017), (ii) seawater at near-bottom conditions (< 100 °C) (e.g., Snow and Dick 1995; Li and Lee 2006); (iii) both H_2O-rich and CO_2-rich fluids released from various layers of a subducting slab (e.g., Bostock et al. 2002; Hamdy et al. 2013); and (iv) hydrothermal fluids infiltrating during and after exhumation (>100 °C) (e.g., Seyfried and Dibble 1980; Li and Lee 2006; Hamdy and Lebda 2007).

The most notable metamorphic process, affecting all the ultramafic rocks in the ED ophiolites, is *serpentinization*, a continuous process of replacement of anhydrous primary silicate minerals by hydrous phyllosilicates (e.g., O'Hanly 1996). Serpentinization reactions have been studied by (1) analysis of vent fluids from peridotite-hosted hydrothermal systems (e.g., Douville et al. 2002), (2) experiments and theoretical considerations (e.g., Allen and Seyfried 2003), and (3) petrographic studies of altered rocks (e.g., Evans 1977; Mével 2003).

The serpentinization of peridotites can occur in low-temperature ($\leq$250 °C) and high-temperature ($\geq$250 °C) environments (Evans 2010). At low temperature, olivine relics tend to retain their original composition, while

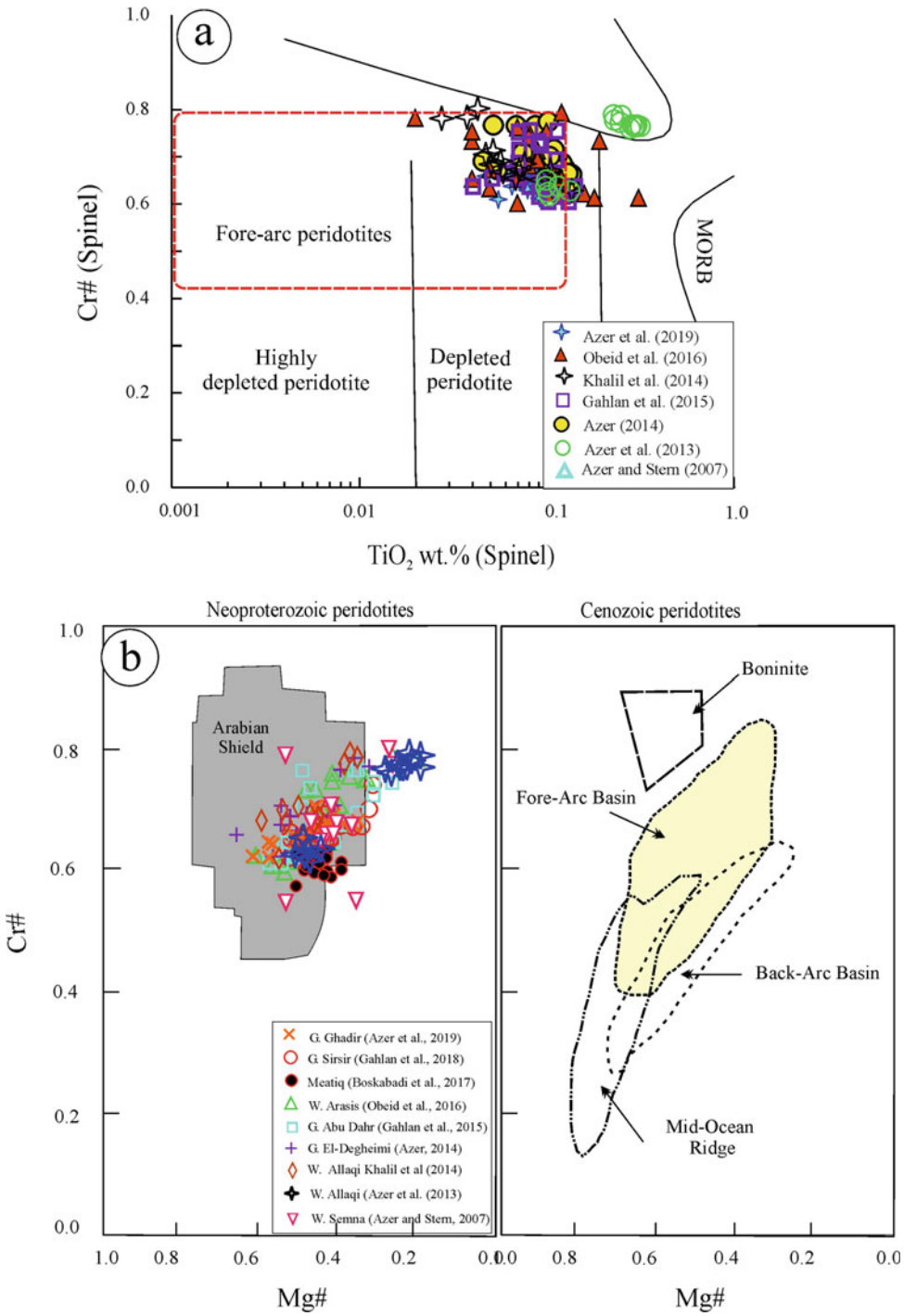

Fig. 12.21 **a** Variation of TiO_2 (wt%) versus Cr# of chromian spinel in ED chromitite, dunite, and harzburgite. Fields of MORB and boninite are after Dick and Bullen (1984) and Arai (1992). Fields of depleted and highly depleted peridotites are after Jan and Windley (1990). Field of fore-arc peridotite (dashed) is after Ohara and Ishii (1998). **b** Comparison, in terms of spinel composition, between the Neoproterozoic ED peridotites and analogous Cenozoic ophiolite fields (Bloomer et al. 1995). The shaded field of the Neoproterozoic ANS peridotites is after Stern et al. (2004). Note that the vast majority of the ED ophiolitic peridotites and the associated chromitites plot in the field of ANS peridotite

high-temperature serpentinization allows interdiffusion of Mg and Fe diffusion, resulting in low Mg# olivine relics coexisting with serpentine. Furthermore, experimental studies have demonstrated that pyroxenes react faster than olivine at temperature above 250–300 °C, but olivine reacts faster than pyroxene at temperature <250 °C (e.g., Martin and Fyfe 1970; Janecky and Seyfried 1986; Allen and Seyfried 2003). In the ED case, olivine appears to have reacted most readily, followed by orthopyroxene and clinopyroxene, and the fresh olivine relics have high Mg# >88. Both features imply low-temperature hydration.

Serpentinization can be isochemical, which requires a significant volume increase and causes fracturing, or allochemical, which can in principle proceed at constant volume as fluids transport Mg^{2+}, Fe^{2+}, Ca^{2+}, and Si^{2+} ions out of the system. Johannes (1969, 1970) provided benchmark

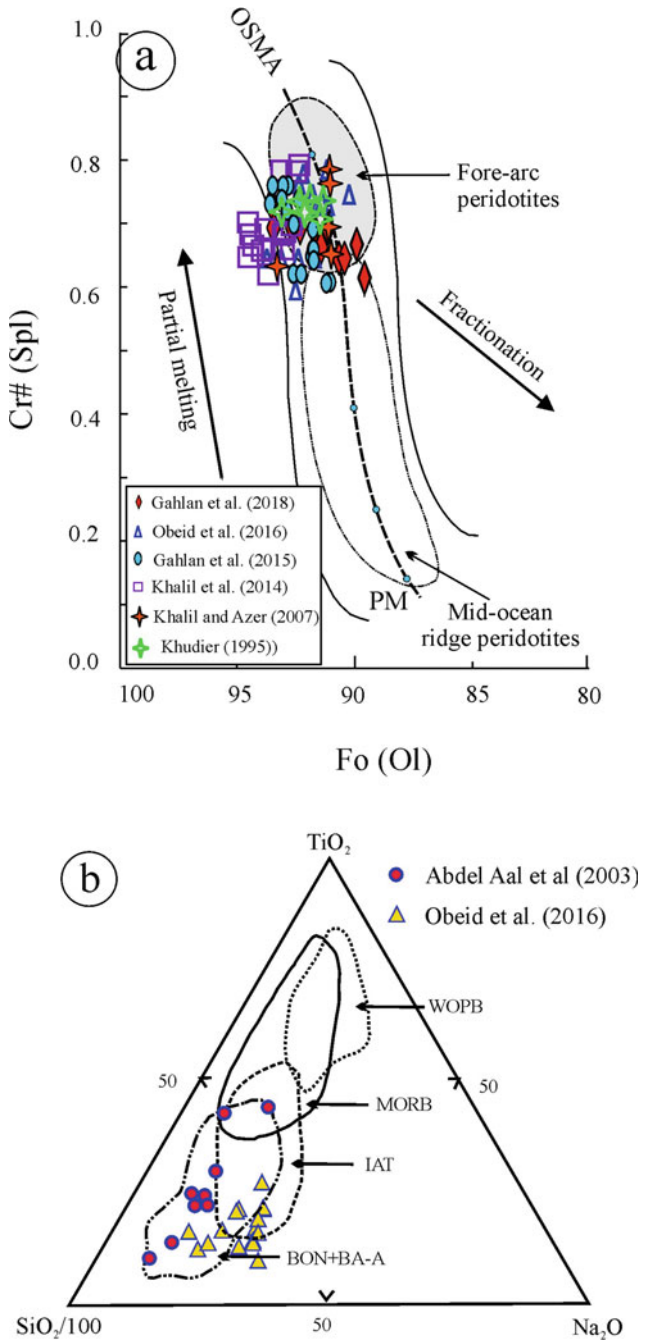

Fig. 12.22 **a** Cr# of spinel versus Fo content of coexisting olivine from serpentinized ED peridotites (Arai 1992). PM: Primitive mantle, OSMA: Olivine–spinel mantle array (Arai 1994a), **b** TiO_2–Na_2O–SiO_2/100 diagram for fresh relics of clinopyroxene in serpentinized ED peridotite (Beccaluva et al. 1989). WOPB = within-ocean plate basalts; MORB = mid-ocean ridge basalts; IAT = island-arc tholeiites; BON + BA-A = boninites + basaltic andesites and andesites from intra-oceanic fore-arcs

experiments of equilibria in the system MgO–SiO_2–H_2O–CO_2 from 0.2 to 1.0 GPa pressure that demonstrates that serpentine coexists only with CO_2-poor fluid phases.

Upon prograde metamorphism, the reverse of serpentinization, i.e., dehydration, can occur, producing metamorphic olivine (e.g., Arai 1975; Evans 1977; Nozaka 2003). Such metamorphic olivine typically lacks chemical zonation or evidence of ductile deformation such as undulatory extinction (e.g., Mercier and Nicolas 1975). Metamorphic olivine has been reported in peridotites from ED ophiolites (e.g., Khalil and Azer 2007; Gahlan 2006) and attributed either to the thermal effects of granitoid intrusions (e.g., Gahlan and Arai 2009; Ahmed et al. 2012b) or to low-pressure high-temperature regional metamorphism (Gahlan et al. 2015a).

During or after serpentinization, many of the ED ophiolite ultramafic rocks were variably deformed and altered to mixtures of serpentine, talc, chlorite, carbonates, and magnetite (e.g., Ghoneim et al. 2003; Farahat 2008; Abdel-Karim et al. 2018; Azer et al. 2019; among others). The timing and fluid sources for events such as carbonatization, listwaenitization, and rodingization are controversial. Recently, Azer et al. (2019) distinguished two stages of carbonation in ED ophiolites. The first stage formed magnesite masses during deep-seated metasomatism and serpentinization, whereas the second stage emplaced carbonate veins after serpentinization, during obduction of the ophiolite. Likewise, listwaenitization in ED ophiolites also took place in two main metasomatic stages, the first associated with the formation of the oceanic crustal section and the second during obduction (Gahlan et al. 2018).

Rodingite is a massive light-colored rock composed of Ca-rich minerals produced by infiltration of Ca-bearing solutions into aureoles around serpentinized ultramafic bodies (Best 2003). Determination of the physical and chemical conditions of rodingite formation, concomitant with serpentinization, can provide detailed information on the effects of ancient seafloor hydrothermal processes and on the tectonic history of an ophiolite. Only a few studies have published data about ED rodingites (Takla et al. 1992; Abdel-Karim 2000; Surour 2019). Although the ED ophiolites have been intensively studied over the last two decades, the associated rodingites have not yet received much attention.

The metamorphic grade implied by the mineral assemblages in serpentinized ultramafic rocks of the ED ranges from greenschist facies (olivine–opx–serpentine–ferritchromite–magnetite) to amphibolite facies (olivine–opx–anthophyllite–talc–tremolite–antigorite–ferritchromite–magnetite) (e.g., Evans and Trommsdorff 1974; Evans 1977; Gahlan et al. 2015a; Obeid et al. 2016). The formation of ferritchromite rims around fresh chrome spinel cores, in particular, indicates greenschist or lower amphibolite facies prograde metamorphism (Evans and Frost 1975; Suita and Streider 1996; Mellini et al. 2005; Azer et al. 2019) with

peak temperatures >500 °C and oxidizing conditions (e.g., Farahat 2008; González-Jiménez et al. 2009).

12.7 Proterozoic Versus Phanerozoic Mantle Sections: A Comparison

Paleoproterozoic (1650–2300 Ma) and Mesoproterozoic (1000–1400 Ma) ophiolites are less abundant globally than Neoproterozoic (543–1000 Ma) examples (Kusky 2004). The Dongwanzi ophiolite (2505 Ma) in north China is considered the world's oldest, nearly complete and well-preserved Paleoproterozoic ophiolite complex (Kusky et al. 2001; Li et al. 2002; Kusky 2004; Huson et al. 2004). Other well-known Paleoproterozoic ophiolites include the Jormua ophiolite (~2000 Ma) of Finland (Peltonen and Kontinen 2004), the Purtuniq ophiolite (1998 Ma) in the Cape Smith Belt of Canada (Scott et al. 1992), and the unique Payson ophiolite (1730 Ma) in the USA (Dann 2004). Recently, some Mesoproterozoic ophiolites have been described from the Karelian Shield of West Africa and from the southwestern USA (e.g., St-Onge et al. 1989; Abouchami et al. 1990; Boher et al. 1992; Dann 2004). By contrast, the youngest ophiolite complex pertaining to the Neoproterozoic era is the Agardagh Tes–Chem ophiolite (570 Ma), Tuva, Central Asia (Pfänder and Kröner 2004). The Arabian–Nubian Shield and the ED of Egypt in particular are rich in well-preserved and exposed Neoproterozoic ophiolites (e.g., Stern et al. 2004 and references therein).

Highly depleted harzburgites with high-Cr# (≥ 0.7) spinel are very common in Proterozoic ophiolites (e.g., Quick 1990; Liipo et al. 1995; Vuollo et al. 1995; Ahmed et al. 2001; Gahlan et al. 2015b; among others). However, similar rocks are not at all uncommon in Phanerozoic ophiolites (e.g., England and Davies 1973; Arai 1997; Tamura et al. 1999; Ishiwatari et al. 2003 and references therein). Likewise, spinel with Cr# as high as 0.8 is commonly found in modern fore-arc regions (e.g., Marian Trench; Ohara and Ishii 1998).

In terms of chromian spinel chemistry, the Neoproterozoic ED ophiolitic peridotites are similar to a number of published Neoproterozoic examples across the Red Sea in the Arabian Shield (Stern et al. 2004 and references therein) (Fig. 12.20b). Like the Arabian Shield peridotites, the ED peridotites are best interpreted in an SSZ setting (e.g., Arai and Yurimoto 1995; Stern et al. 2004).

Overall, the association harzburgite–dunite–chromitite in the Neoproterozoic ED ophiolites and in Phanerozoic cases is similar in their field, petrographic and mineral chemical characteristics (Fig. 12.22). The formation process of podiform chromitites in ED ophiolites is therefore probably similar to that in Phanerozoic cases, namely, by melt–peridotite interaction and subsequent melt mixing in an SSZ setting (e.g., Ahmed et al. 2001). Comparing the spinel chemistry of the Neoproterozoic ED chromitites with a compilation of Phanerozoic equivalents, we find that the most notable difference is modestly but systematically lower TiO_2 in the ED cases. This can be attributed to somewhat higher degrees of partial melting or a more fractional character of melting in development of the Neoproterozoic examples (Kelemen et al. 1995; Asimow and Stolper 1999). In general, however, the Neoproterozoic ophiolites support the notion that subduction processes have on the whole been unchanged over the last billion years of Earth history. No dramatic differences stand out that require a non-uniformitarian interpretation of these rocks.

12.8 Mineralization

The mantle sections of ophiolites are worthy targets for mining and exploration. They host a variety of ores (chromite, gold, and iron–nickel laterites) and industrial minerals (talc, asbestos, and serpentine) (e.g., Coleman 1977; Klemm and Klemm 2013; Gahlan et al. 2018; Fu et al. 2019; among others). In the ED, in particular, there is a strong association between ophiolites and mineralization, including chromite, talc, asbestos, platinum-group elements, Cu–Ni–Co, magnesite, and gold (Klemm et al. 2001; Kusky and Ramadan 2002; Ahmed and Hariri 2008; Azer et al. 2019). We will discuss some of the major resource types in the following sections.

12.8.1 Chromitite

Chromite deposits in Egypt are commonly hosted by serpentinized ultramafic rocks, widely distributed in the central and southern ED. In most cases, chromitites occur as lenticular bodies of variable size, from thin pencil-shaped layers (a few centimeters long) to large pods (up to 30 m along strike). The average pod is relatively small (≤ 5 m length and ≤ 2 m width). The podiform chromitites (Thayer 1964) are not especially abundant in the ED mantle sections as a whole and are commonly concentrated in the shallowest parts, closest to the petrologic Moho (e.g., Hume 1937; Amin 1948; Takla et al. 1975; Takla and Noweir 1980; El Haddad and Khudeir 1989; Ahmed et al. 2001; Gahlan et al. 2015b; among others). They are commonly concordant to sub-concordant with the plano-linear fabrics of the host rocks and enveloped by dunite those grades outward to harzburgite (Fig. 12.2). Ore pods range massive, nodular, anti-nodular, and disseminated textures are observed.

The ED chromitites are mostly of metallurgical-grade ($Cr_2O_3 > 40$ wt% and $Al_2O_3 < 20$ wt%). Notably, the

South ED chromitites are more refractory (i.e., Cr-rich) than the Central ED examples. Arai (1997) concluded that size of chromitite pods is highly dependent on the chemistry of the host peridotites, particularly spinel Cr#. Globally, the largest chromitite pods are hosted by moderately refractory peridotite host (spinel Cr# = 0.4–0.6), whereas only very small chromitite pods, if any, are typically hosted either by cpx-free highly refractory peridotites (spinel Cr# > 0.7) or by lherzolitic peridotites (spinel Cr# $\leq$ 0.3). As the ED host peridotites are all of the highly refractory variety, the low overall size and abundance of podiform chromitites in the ED mantle sections appear consistent with the tendency proposed by Arai (1997). Like podiform chromitites worldwide, those of the ED mantle section are well explained as the result of melt–peridotite interaction and subsequent melt mixing in the SSZ upper mantle (e.g., Lago et al. 1982; Paktunc 1990; Arai and Yurimoto 1994, 1995; Zhou et al. 1994, 1996; Arai 1997; Ahmed et al. 2001; Ahmed 2013; Azer et al. 2019).

12.8.2 Gold

Prospects and productive gold mining sites are widespread in the ED mantle sections (Fig. 12.23), particularly in the carbonatized serpentinites (e.g., Botros 2002, 2004; Zoheir and Lehmann 2011; Abd El-Rahman et al. 2012a; Boskabadi et al. 2017; Gahlan et al. 2018). Gold mining in these areas extends back to Pharaonic times (Harraz 2000; Klemm and Klemm 2013). According to Botros (2004), the El-Sid gold deposit is a good example of vein-type mineralization hosted in sheared ophiolitic ultramafic rocks. The El-Sid gold mine is confined to hydrothermal quartz veins at the contact between granite and serpentinite except for extensions into the serpentinite along a thick zone of graphite schist (El-Bouseily et al. 1985). Historically worked gold deposits are associated with ophiolitic rocks in the Wadi Allaqi region.

During serpentinization and metamorphism, gold behaves, to some extent, like the fluid-mobile elements (B, Li, S, As, Rb, Sr, Sb, Cs, Ba, Pb, and U) (e.g., Deschamps et al. 2013; Gahlan et al. 2018; and references therein). Typically, gold concentrations are ~1 ppb in depleted mantle (Salters and Stracke 2004), about 2.8 ppb in average ophiolitic rocks (Crocket 1991), and ~3–5 ppb in serpentinites (Buisson and Leblanc 1987). The Fawakhir goldmine shows gold concentrations up to ~30 g/ton (Hussein 1990), supporting the suggestion of Buisson and Leblanc (1987) that Neoproterozoic ophiolitic mantle sections are modestly enriched in gold. Abd El-Rahman et al. (2012b) noted the dominance of vein-type gold deposits along the eastern side of the NW-trending Najd Fault System and attributed this pattern to the abundance of serpentinite bodies in the arc–fore-arc belt.

A spatial and genetic relationship has been observed between carbonated ultramafic rocks, subsequent granite intrusions, and gold mineralization. Listvenites are considered a prime target for gold prospecting in ophiolites (Botros 2004; Ahmed and Hariri 2008). For example, the listvenites at G. Sirsir show gold concentrations up to 6584 ppb (as well as As and Ag enrichment) (Gahlan et al. 2018). Azer (2008) extended this association into a genetic link between gold mineralization and carbonate alteration of ED ophiolites, whereby carbonatization preconcentrates gold up to 1,000 times compared to the original ultramafic rocks and interaction with hydrothermal systems associated with granite intrusions further concentrates and remobilizes gold (Cox and Singer 1986; Azer 2008). However, the relation between Au en-richment and the carbonatization process is controversial (e.g., Azer 2013; Boskabadi et al. 2017; Gahlan et al. 2018; and references therein).

A variety of potential minerals has been proposed to host gold in serpentinites including nickel sulfides (e.g., Takla and Surour 1996; Khalil et al. 2003; Emam and Zoheir 2013), Cu–Fe–Ni sulfides (e.g., Ferraris and Lorand 2015), olivine (Au as nano-inclusions), and lizardite (Boskabadi et al. 2017). Breakdown of these Au-bearing minerals upon infiltration of CO_2-bearing hydrothermal fluids liberates fluid-mobile elements and results in an Au-bearing CO_2-rich fluid phase. The source of CO_2-rich hydrothermal fluid phase has been a matter of debate, but a mixture of mantle-derived and surface-derived CO_2 has been widely accepted (Boskabadi et al. 2017; Gahlan et al. 2018; and references therein).

It has been proposed that the contrast in rheology and permeability between listvenites and its country rocks then promotes precipitation of gold at their interfaces (e.g., Zoheir and Lehmann 2011; Azer 2013; Zoheir and Moritz 2014; Boskabadi et al. 2017; Gahlan et al. 2018). This mechanism is most favored at greenschist facies metamorphic conditions, where brittle–ductile deformation is available to form pathways for gold mineralization (El-Gaby et al. 1988; Botros 2004). The result is development of auriferous quartz veins within sheared serpentinites and listvenites (e.g., Zoheir and Lehmann 2011; Abd El-Rahman et al. 2012b). The auriferous veins are composed mainly of quartz and carbonates with subordinate sulfides (mainly pyrite and chalcopyrite) (Botros 2002, 2004). Gold occurs either as native, tiny specks within quartz veins or as inclusions in sulfides, particularly in pyrite and arsenopyrite (Abd El-Rahman et al. 2012a).

12.8.3 Talc–Carbonates

Worldwide production of talc has increased from 7.4 million tons in 2011 to about 10 million tons in 2018. The major

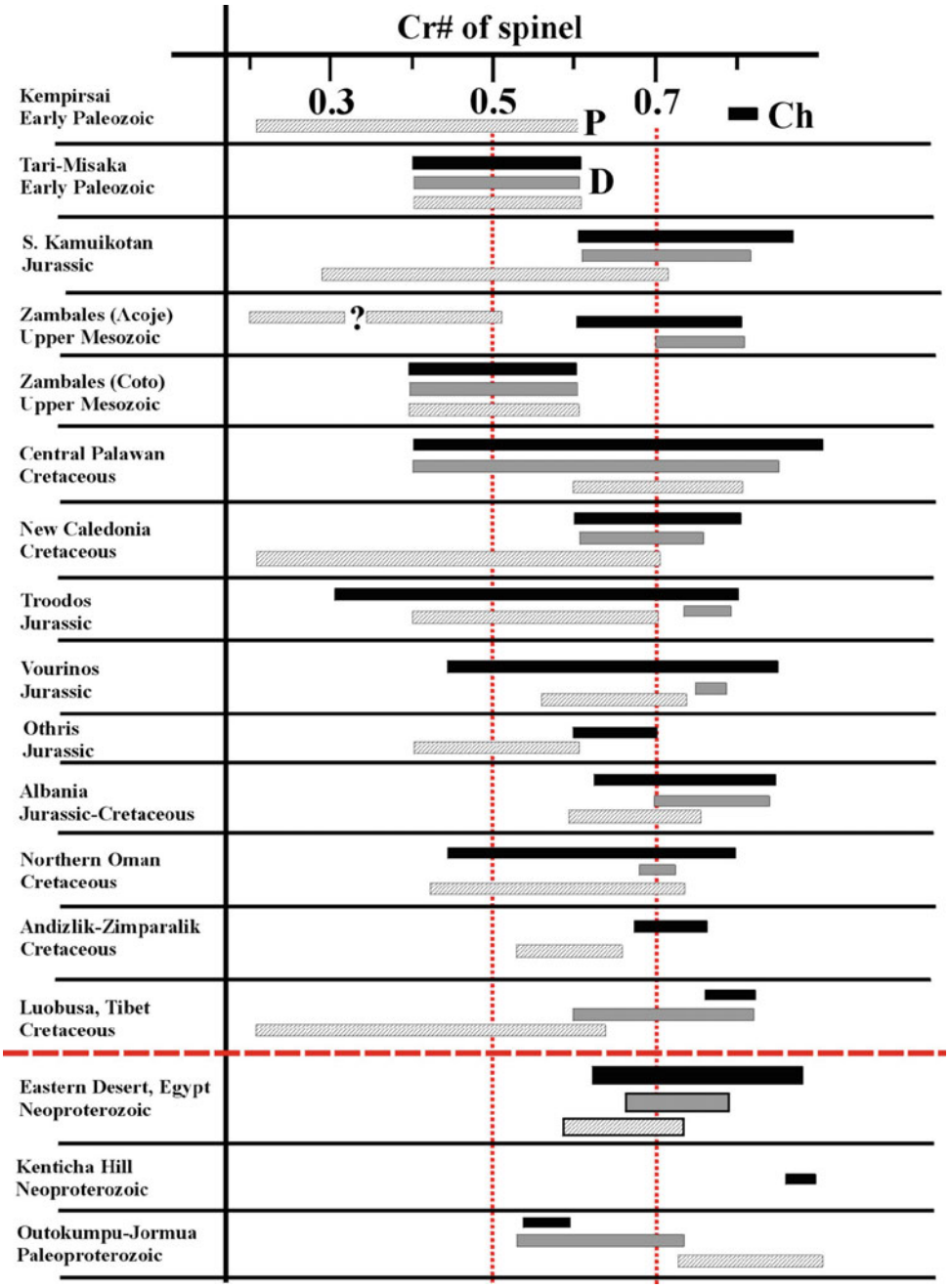

Fig. 12.23 Comparison between Proterozoic and Phanerozoic ophiolitic peridotite (P), dunite (D), and chromitite (Ch), in terms of spinel composition. The Phanerozoic ophiolite data are from Arai (1997) and references therein; the Kenticha Hill chromitite data are from Bonavia et al. (1993), the Outokumpu Jormua ophiolite data are after Liipo et al. (1995), and Egyptian ED data are from Ahmed et al. (2001) and Gahlan (2015a)

producing countries are China, USA, Finland, and France. Egypt produced 12,924 tons of talc in 2011 and about 172,181 tons in 2015. The Darhib and Atshan deposits have been the most intensively exploited to date. Talc was mined and used by ancient Egyptians for beads and for cosmetic vessels in both the Middle and New Kingdoms. High-purity talc (>95%) is used in cosmetics, steatite, cordierite ceramics, paper, and plastics. Medium purity talc (75–95%) is used in paper, plastics, wall tiling, paint, and rubber. Low-purity talc (e.g., <75%) is used in paint, roofing materials, flooring, and fertilizers.

Talc–carbonate rocks are widely distributed at various ED localities. Economically significant deposits of talc are already being mined along the suture in the Wadi Allaqi region, but huge quantities of practically untapped talc–carbonate rocks could serve as an important potential source of magnesia for strategic industries such as refractory ceramics and electrical insulators. There are two types of talc–carbonate deposits in the ED: (1) talc–carbonates associated with volcano-sedimentary rocks of island-arc stage, and (2) talc–carbonates associated with ophiolitic ultramafic rocks. Talc–carbonates associated with ophiolitic

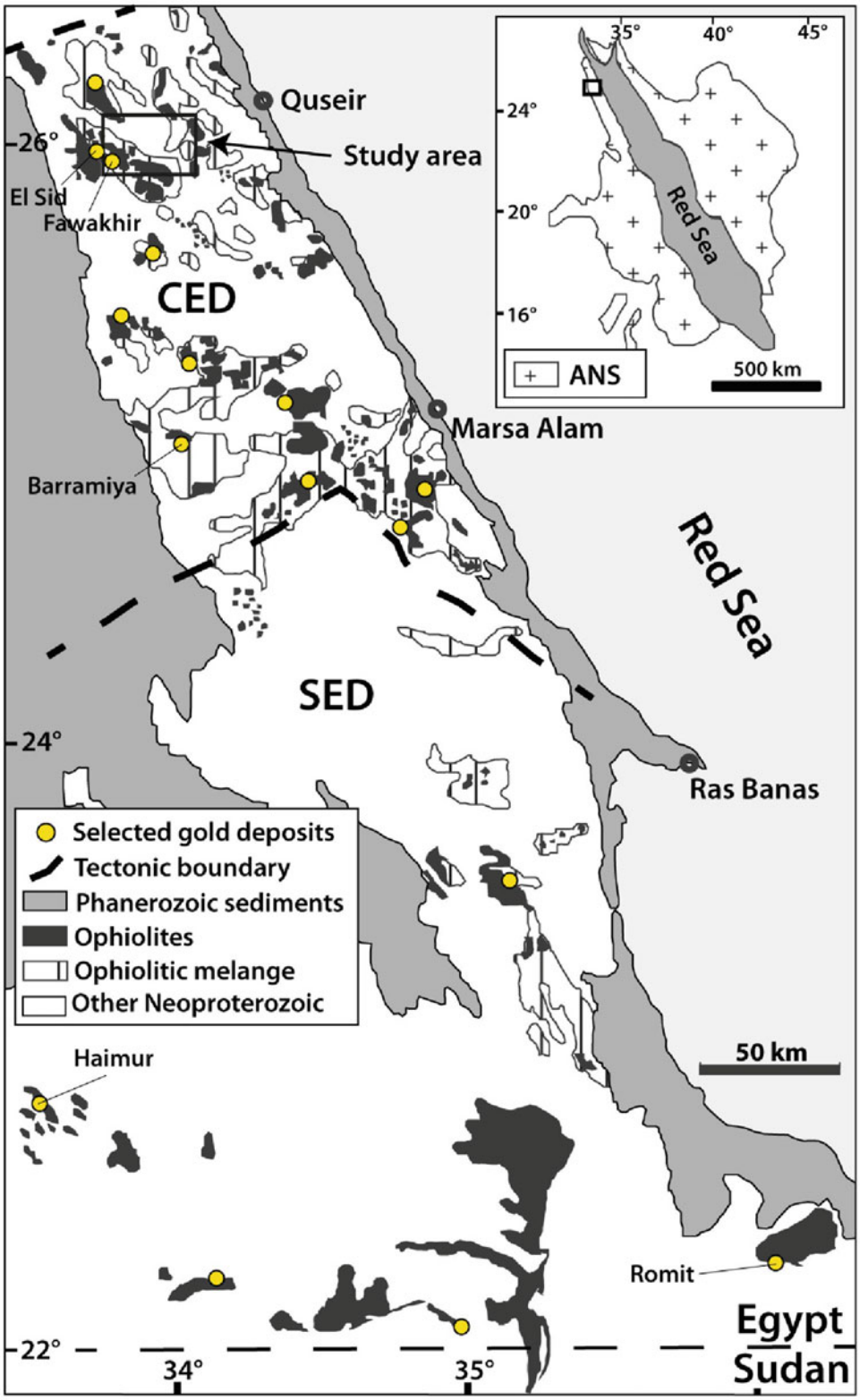

Fig. 12.24 Simplified geological map showing the extent of the ANS (inset), the distribution of ophiolitic bodies, and selected Au deposits in the Egyptian segment of ANS

rocks are well developed in the Barramiya, Atud, and Atalla areas. These rocks were called Barramiya rocks (Hume 1934; Rittmann 1958). They occur either as separate bodies or associated with serpentinite. They are developed along major faults and shear zones cutting serpentinite units or at thrust contacts between obducted serpentinites and other country rocks of island-arc affinity.

As discussed above, talc–carbonate rocks associated with the serpentinites are easily recognized by their distinct appearance in the field. A systematic campaign is needed to map the occurrences of talc–carbonates in Egypt and to classify them according to standard industrial specifications in order to locate the highest-purity deposits (suitable for ceramic applications) and to define Egypt's reserves of talc.

12.8.4 Magnesite

Reaction between CO_2-rich fluids and olivine or serpentine usually produces the industrially useful mineral magnesite ($MgCO_3$) (e.g., Klein et Garrido 2011), which is commonly found worldwide in networks of veins in the ultramafic parts of ophiolite sequences. In the ED, both massive pods of magnesite and very high-purity magnesite veins have been described at numerous ophiolite-associated localities (Azer et al. 2019). The massive magnesites, as discussed above, are formed by replacement during early serpentinization processes, whereas the vein-type magnesite is formed later. The magnesite veins fill fractures and cavities in serpentinites (e.g., Salem et al. 1997; Ghoneim 2003; Ghoneim et al. 1999).

12.8.5 Serpentinite

Serpentinite itself is a decorative and industrial rock that can be used, for example, for neutron shielding in nuclear reactors (e.g., Abulfaraj and Kamal 1994). The mineralogy, color, and mechanical properties determine whether given serpentinites have decorative or industrial value. Streaks of associated minerals such as talc and carbonates for attractive visual patterns that are considered controlling factors in the value of serpentinites as ornamental stones (e.g., Ismael and Hassan 2008). They are many serpentinite quarries in the ED; the largest one is the Wadi Sodmein quarry (Figs. 12.24 and 12.25).

12.9 Conclusions

- The mantle sections or lower units of ophiolites in the Eastern Desert of Egypt generally form massive ridges and sheet-like bodies of serpentinized harzburgite, dunite, and rarely lherzolite with chromitite pods and ultramafic cumulates. They are fault-bounded and often well preserved in the troughs of major synforms. The contacts

Fig. 12.25 Serpentinite quarry in Wadi Sodmein showing cut surfaces of Atg-serpentinite

between the mantle and crustal sections of these ophiolites were originally magmatic but are now inevitably disrupted by tectonism.

- Petrographic examination shows that almost all primary silicates are typically replaced, except for chromian spinel and rare relics of olivine and sometimes pyroxene.
- Regional metamorphism to greenschist or amphibolite facies and CO_2-metasomatism resulted in an array of talc–carbonate, listvenite, magnesite, and carbonate-bearing meta-ultramafic rocks.
- The modal mineralogy (i.e., low or zero abundance of clinopyroxene), mineral chemistry (high-Cr#, low-TiO_2 spinel; high Fo and NiO in relict olivine; low Al2O3 in relict orthopyroxene), and whole-rock chemistry (high-Mg#; enrichment of Ni, Cr, and Co; depletion of Al_2O_3, TiO_2, and CaO; depleted and unfractionated REE patterns) of the ED mantle rocks all point to highly refractory protoliths that experienced high degrees of partial melt extraction. In all these regards, they resemble modern fore-arc peridotites.
- The ED podiform chromitites resemble their Phanerozoic equivalents and may have been formed by the same mechanisms. In general, the ED Neoproterozoic ophiolite mantle sections closely resemble Phanerozoic fore-arc equivalents, suggesting little change in the geothermal and tectonic regime of Earth's subduction zones since the Late Proterozoic era.
- A variety of economically viable deposits of ore (e.g., chromite and gold) and industrial (e.g., asbestos, talc, magnesite, and serpentinite) minerals are spatially associated with ED mantle sections.

Acknowledgement Hisham A. Gahlan owes the debt of gratitude to Assiut University, as well as King Saud University, Deanship of Scientific Research for their support.

References

Abd El-Rahman Y, Helmy HM, Shibata T, Yoshikawa M, Arai S, Tamur A (2012a) Mineral chemistry of the Neoproterozoic Alaskan-type Akarem Intrusion with special emphasis on amphibole: implications for the pluton origin and evolution of subduction-related magma. Lithos 155:410–425

Abd El-Rahman Y, Polat A, Dilek Y, Fryer B, El-Sharkawy M, Sakran S (2009a) Geochemistry and tectonic evolution of the Neoproterozoic Wadi Ghadir ophiolite, Eastern Desert. Egypt Lithos 113:158–178

Abd El-Rahman Y, Polat A, Dilek Y, Fryer BJ, El-Sharkawy M, Sakran S (2009b) Geochemistry and tectonic evolution of the Neoproterozoic incipient arc-fore-arc crust in the Fawakhir area, Central Eastern Desert of Egypt. Precamb Res 175:116–134

Abd El-Rahman Y, Polat A, Dilek Y, Kusky TM, El-Sharkawi M, Said A (2012b) Cryogenian ophiolite tectonics and metallogeny of the central eastern desert of Egypt. Int Geol Rev 54:1870–1884

Abdel Aal AY, Farahat ES, Hoinken G, El-Mahallawi MM (2003) Ophiolites from the Egyptian shield: a case for a possible inter-arc origin. Mitt Oesterr Ges 148:81–83

Abdel Khalek ML, Takla MA, Sehim A, Hamimi Z, El Manawi AW (1992) Geology and tectonic evolution of Wadi Beitan area, south Eastern Desert, Egypt. In: International conference geology. The Arab World, Cairo University, Egypt (GAW1), pp 369–393

Abdel-Karim AAM (2000) Chlorite schists and rodingites in the mafic-ultramafic rocks from the central eastern desert of Egypt: petrogenesis and metamorphic history. M.E.R.C. Ain Shams University, Earth Science Series 14:150–170

Abdel-Karim AAM, Ali S, El-Shafei SA (2018) Mineral chemistry and geochemistry of ophiolitic metaultramafics from Um Halham and Fawakhir, Central Eastern Desert. Egypt Intern J Earth Sci 107:2337–2355

Abdel-Karim AAM, El-Mahallawi MM, Finger F (1996) The ophiolite mélange of Wadi Dunqash and Arayis, Eastern Desert of Egypt: petrogenesis and tectonic evolution. Acta Mineral Petrogr Szaged 37:129–141

Abdelsalam MG, Abdeen MM, Dowaidar HM, Stern RJ, Abdelghaffar AA (2003) Structural evolution of the Neoproterozoic Western Allaqi-Heiani suture, southeastern Egypt. Precamb Res 124:87–104

Abdelsalam MG, Gao SS, Liégeois J-P (2011) Upper mantle structure of the Saharan metacraton. J Afr Earth Sci 60:328–336

Abo-Soliman MY (2019) Deformation history, kinematic setting and microstructural analysis of some major shear zones and related structures in Najd Fault Corridor, Eastern Desert, Egypt, Ph.D. Thesis, Aswan University, p 537

Abouchami W, Boher M, Michard A, Albarède F (1990) A major 2.1 Ga event of mafic magmatism in west Africa: An early stage of crustal accretion. J Geophys Res 95:17605–17629

Abulfaraj WH, Kamal SM (1994) Evaluation of ilmenite serpentine concrete and ordinary concrete as nuclear reactor shielding. Radiat Phys Chem 44:139–148

Ahmed AH (2013) Highly depleted harzburgite–dunite–chromitite complexes from the Neoproterozoic ophiolite, south Eastern Desert, Egypt: a possible recycled upper mantle lithosphere. Precamb Res 233:173–192

Ahmed AH, Arai S, Attia AK (2001) Petrological characteristics of podiform chromitites and associated peridotites of the Pan African ophiolite complexes of Egypt. Mineral Deposit 36:72–84

Ahmed AH, Gharib M, Arai S (2012a) Characterization of the thermally metamorphosed mantle–crust transition zone of the Neoproterozoic ophiolite at Gebel Mudarjaj, south Eastern Desert. Egypt Lithos 142–143:67–83

Ahmed AH, Harbi HM, Habtoor AM (2012b) Compositional variations and tectonic settings of podiform chromitites and associated ultramafic rocks of the Neoproterozoic ophiolite at Wadi Al Hwanet, northwestern Saudi Arabia. J Asian Earth Sci 56:118–134

Ahmed Z, Hariri MM (2008) Neoproterozoic ophiolites as developed in Saudi Arabia and their oceanic and pericontinental domains. Arab J Sci Eng 33:17–54

Ali K, Azer M, Gahlan H, Wilde S, Samuel M, Stern R (2010) Age constraints on the formation and emplacement of Neoproterozoic ophiolites along the Allaqi-Heiani Suture, South Eastern Desert of Egypt. Gondwana Res 18(4):583–595

Ali KA, Andresen A, Manton WI, Stern RJ, Omar SA, Maurice AE (2012) U-Pb zircon dating and Sr–Nd–Hf isotopic evidence to support a juvenile origin of the ~634 Ma El Shalul granitic gneiss dome. Arabian-Nubian Shield Geol Mag 149(5):783–797

Allan JF, Dick HJB (1996) Cr-rich spinel as a tracer for melt migration and melt-wall interaction in the mantle: Hess Deep, Leg 147. In: Mével C, Gillis KM et al (eds), Proceedings of the Ocean Drilling Program, Scientific Results 147. College Station, TX: Ocean Drilling Program, pp 157–172

Allen DE, Seyfried WEJ (2003) Compositional controls on vent fluids from ultramafic-hosted hydrothermal systems at mid-ocean ridges: An experimental study at 400 °C, 500 bars. Geochim Cosmochim Acta 67(8):1531–1542

Amin MS (1948) Origin and alteration of chromite from Egypt. Econ Geol 43:133–153

Andresen A, El-Rus MAA, Myhre PI, Boghdady GY, Corfu F (2009) U-Pb TIMS age constraints on the evolution of the Neoproterozoic Meatiq Gneiss Dome, Eastern Desert, Egypt. Int J Earth Sci 98: 481–497

Anonymous (1972) Penrose field conference on ophiolites. Geotimes 17:24–25

Arai S (1975) Contact metamorphosed dunite–harzburgite complex in the Chugoku district, western Japan. Contrib Mineral Petrol 52:1–16

Arai S (1980) Dunite-harzburgite-chromitite complexes as refractory residue in the Sangun-Yamaguchi zone, western Japan. J Petrol 21:141–165

Arai S (1992) Chemistry of chromian spinel in volcanic rocks as a potential guide to magma chemistry. Mineral Mag 56:173–184

Arai S (1994a) Compositional variation of olivine–chromian spinel in Mg-rich magmas as a guide to their residual spinel peridotites. J Volcanol Geotherm Res 59:279–293

Arai S (1994b) Characterization of spinel peridotites by olivine-spinel compositional relationships: review and interpretation. Chem Geol 113(3–4):191–204

Arai S (1997) Control of wall-rock composition on the formation of podiform chromitites as a result of magma/peridotite interaction. Resour Geol 47:177–187

Arai S, Matsukage K (1996) Petrology of the gabbro–troctolite–peridotite complex from Hess Deep, Equatorial Pacific: implications for mantle–melt interaction within the oceanic lithosphere. In: Mével C, Gillis KM et al (eds), Proceedings of the Ocean Drilling Program, Scientific Results 147. College Station, TX: Ocean Drilling Program, pp 135–155

Arai S, Yurimoto H (1994) Podiform chromitites of Tari-Misaka ultramafic complex, Southwest Japan, as mantle-melt interaction products. Econ Geol 89:1279–1288

Arai S, Yurimoto H (1995) Possible sub-arc origin of podiform chromitites. Island Arc 4:104–111

Arif M, Jan MQ (2006) Petrotectonic significance of the chemistry of chromite in the ultramafic-mafic complexes of Pakistan. J Asian Earth Sci 27:628–646

Asimow PD, Stolper EM (1999) Steady-state mantle-melt interactions in one dimension: I. Equilibrium transport and melt focusing. J Petrol 40(3): 474–494

Azer MK (2008) Origin of Neoproterozoic Ophiolitic Serpentinites and Their Economic Potentialities, Eastern Desert, Egypt. 33th International Geological Congress, Oslo-Norway (Abstract)

Azer MK (2013) Evolution and economic significance of listwaenites associated with Neoproterozoic ophiolites in south Eastern Desert. Egypt Geologica Acta 11:113–128

Azer MK, Asimow PD (this volume) Petrogenetic evolution of the Neoproterozoic igneous rocks of Egypt

Azer MK, Gahlan HA, Asimow PD, Mubarak HS, Al-Kahtany KM (2019) Multiple stages of carbonation and element redistribution during formation of ultramafic-hosted magnesite in Neoproterozoic ophiolites of the Arabian-Nubian Shield. Egypt J Geol 127:81–107

Azer MK, Khalil AES (2005) Petrological and mineralogical studies of Pan-African serpentinites at Bir Al-Edeid area. Central Eastern Desert. Egypt J Afr Earth Sci 43:525–536

Azer MK, Samuel MD, Ali KA, Gahlan HA, Stern RJ, Ren M, Moussa HE (2013) Neoproterozoic ophiolitic peridotites along the Allaqi-Heiani Suture, South Eastern Desert. Egypt Mineral Petrol 107:829–848

Azer MK, Stern RJ (2007) Neoproterozoic (835-720 Ma) serpentinites in the Eastern Desert, Egypt: fragments of fore-arc mantle. J Geol 115:457–472

Bakor AR, Gass IG, Neary CR (1976) Jabal Al Wask, northwest Saudi Arabia: an Eocambrian back-arc ophiolite. Earth Planet Sci Lett 30:1–9

Barnes SJ, Roeder PL (2001) The range of spinel composition in terrestrial mafic ultramafic rocks. J Petrol 42:2279–2302

Beccaluva L, Coltorti M, Giunta G, Siena F (2004) Tethyan vs. Cordilleran ophiolites: a reappraisal of distinctive tectono-magmatic features of supra-subduction complexes in relation to the subduction mode. Tectonophysics 393(1–4):163–174

Beccaluva L, Macciotta G, Piccardo G, Zeda O (1989) Clinopyroxene composition of ophiolite basalts as petrogenetic indicator. Chem Geol 77(3–4):165–182

Bédard J (1999) Petrogenesis of boninites from the Betts Cove ophiolite, Newfoundland, Canada: identification of subducted source components. J Petrol 40(12):1853–1889

Best MG (2003) Igneous and metamorphic petrology. Blackwell Science Ltd., Oxford

Boher M, Abouchami W, Michard A, Albarède A, Arndt NT (1992) Crustal growth in West Africa at 2.1 Ga. J Geophys Res 97:345–369

Bonatti E, Michael PJ (1989) Mantle peridotites from continental rifts to ocean basins to subduction zones. Earth Planet Sci Lett 91:297–311

Bonavia FF, Diella V, Ferrario A (1993) Precambrian Podiform Chromitites from Kenticha Hill, southern Ethiopia. Econ Geol 88:198–202

Boskabadi A, Pitcairn IK, Broman C, Boyce A, Teagle DAH, Cooper MJ, Azer MK, Mohamed FH, Stern RJ, Majka J (2017) Carbonate alteration of ophiolitic rocks in the Arabian-Nubian Shield of Egypt: sources and compositions of the carbonating fluid and implications for the formation of Au deposits. Inter Geol Rev 59(4):391–419

Bostock MG, Hyndman RD, Rondenay S, Peacock SM (2002) An inverted continental Moho and serpentinization of the forearc mantle. Nature 417:536–538

Botros NS (2002) Metallogeny of gold in relation to the evolution of the Nubian Shield in Egypt. Ore Geol Rev 19:137–164

Botros NS (2004) A new classification of the gold deposits of Egypt. Ore Geol Rev 25:1–37

Buisson G, Leblanc M (1987) Gold in mantle peridotites from Upper Proterozoic ophiolites in Arabia, Mali and Morocco. Econ Geol 82:2091–2097

Coish RA, Gardner P (2004) Suprasubduction-zone peridotite in the northern USA Appalachians: evidence from mineral composition. Miner Mag 68:699–708

Coleman RG (1971) Plate tectonic emplacement of upper mantle peridotite along continental edges. J Geophys Res 76:1212–1222

Coleman RG (1977) Ophiolites: ancient oceanic lithosphere?. Springer-Verlag, Berlin Heidelberg New York, p 229

Coleman RG, Keith TE (1971) A chemical study of serpentinization—Burro Mountain, California. J Petrol 12:311–328

Crocket JH (1991) Distribution of gold in the Earth's crust. In: Foster RP (ed) Gold Metallogeny and Exploration. Blackie, Glasgow, pp 1–36

Dann JC (2004) The 1.73 Ga Payson ophiolite, Arizona, USA. In: Kusky TM (ed) Precambrian ophiolites and related rocks. Elsevier, Amsterdam, pp 73–94

Deschamps F, Godard M, Guillot S, Hattori K (2013) Geochemistry of subduction zone serpentinites. A Review Lithos 178:96–127

Dick HJB (1977) Partial melting in the Josephine peridotite I, the effect on mineral composition and its consequence for geobarometry and geothermometry. Amer J Sci 277:801–832

Dick HJB, Bullen T (1984) Chromian spinel as a petrogenetic indicator in abyssal and Alpine-type peridotites and spatially associated lavas. Contrib Mineral Petrol 86:54–76

Dilek Y, Newcomb S (2003) Ophiolite concept and the evolution of geological thought. Geol Soc Amer Spec Paper 373: 504

Dixon TH (1979) The evolution of continental crust in the Late Precambrian Egyptian Shield. Ph.D. Thesis, Univ California San Diego, p 231

Donaldson MJ (1981) Redistribution of ore elements during serpentinization and talc–carbonate alteration of some Archean dunites, Western Australia. Econ Geol 76:1698–1713

Douville E, Charlou JL, Oelkers EH, Bienvenu P, Jove Colon CF, Donval JP, Fouquet Y, Prieur D, Appriou P (2002) The rainbow vent fluids (36°14' N, MAR): the influence of ultramafic rocks and phase separation on trace metal contents on Mid-Atlantic Ridge hydrothermal fluids. Chem Geol 184:37–48

Downes H (2001) Formation and modification of the shallow sub-continental lithospheric mantle: a review of geochemical evidence from ultramafic xenolith suites and tectonically emplaced ultramafic massifs of Western and Central Europe. J Petrol 42:223–250

El Bayoumi RM (1983) Ophiolites and mélange complex of Wadi Ghadir Area, Eastern Desert. Egypt Bull Inst Appl Geol King Abdul Aziz Univ Jeddah 6:329–342

El Sharkawy MA, El Bayoumi RM (1979) The ophiolites of Wadi Ghadir area, Eastern Desert. Egypt Ann Geol Surv Egypt 9:125–135

El-Bouseily AM, El-Dahhar MA, Arslan AI (1985) Ore-microscopic and geochemical characteristics of gold-bearing sulfide minerals, El Sid Gold mine, Eastern Desert. Egypt Mineral Deposit 20:194–200

El-Gaby S, List FK, Tehrani R (1988) Geology, evolution and metallogenesis of the Pan-African Belt in Egypt. In: El-Gaby S, Greiling RO (eds) The Pan-African Belt of northeast Africa and adjacent areas. Vieweg, Braunschweig, pp 17–68

El-Gaby S, List FK, Tehrani R (1990) The basement complex of the Eastern Desert and Sinai. In: Said R (ed) The geology of Egypt. Balkema, Rotterdam, pp 175–184

El-Haddad MA, Khudeir AA (1989) Geological and geochemical studies on some chromite deposits, central Eastern Desert. Egypt Bull Fac Sci Assiut Univ 13:141–158

El-Sayed MM, Furnes H, Mohamed FH (1999) Geochemical constraints on the tectonomagmatic evolution of the late Precambrian Fawakhir ophiolite, Central eastern Desert. Egypt J Afr Earth Sci 29:515–533

Emam A, Zoheir B (2013) Au and Cr mobilization through metasomatism: microchemical evidence from ore bearing listvenite, South Eastern Desert of Egypt. J Geochem Explor 125:34–45

England RN, Davies HL (1973) Mineralogy of ultramafic cumulates and tectonites from eastern Papua. Earth Planet Sci Lett 17:416–425

Evans BW (1977) Metamorphism of Alpine peridotites and serpentinites. Ann Rev Earth Planet Sci 5:397–447

Evans BW (2010) Lizardite versus antigorite serpentinite: magnetite, hydrogen, and life (?). Geology 38:879–882

Evans BW, Trommsdorff V (1974) Stability of enstatites + talc, and CO_2-metasomatism of metaperidotite, Val d'efra, Lepontine Alps. Amer J Sci 274:274–296

Evans WB, Frost BR (1975) Chrome-spinel in progressive metamorphism–a preliminary analysis. Geochim Cosmochim Acta 39:959–972

Farahat ES (2008) Chrome-spinels in serpentinites and talc carbonates of the El Ideid-El-Sodmein District, central Eastern Desert, Egypt: their metamorphism and petrogenetic implications. Chem Erde 68:193–205

Farahat ES (2010) Neoproterozoic arc-back-arc system in the central Eastern Desert of Egypt: evidence from supra-subduction zone ophiolites. Lithos 120:293–308

Farahat ES, El Mahallawi MM, Hoinkes G, Abdel Aal AY (2004) Continental back-arc basin origin of some ophiolites from the Eastern Desert of Egypt. Mineral Petrol 82:81–104

Ferraris C, Lorand J-P (2015) Novodneprite ($AuPb_3$), anyuiite [$Au(Pb, Sb)_2$] and gold micro- and nano-inclusions within plastically deformed mantle-derived olivine from the Lherz peridotite (Pyrenees, France): a HRTEM–AEM–EELS study. Phys Chem Miner 42:143–150

Francis GH (1956) The serpentinite mass in Glen Urquhart, Inverness-shire, Scotland. Amer J Sci 254:201–226

Fu W, Feng Y, Luo P, Zhang Y, Huang X, Zeng X, Cai Q, Zhou Y (2019) Weathering of Ophiolite Remnant and Formation of Ni Laterite in a Strong Uplifted Tectonic Region (Yuanjiang, Southwest China). Minerals 9:51

Furnes H, de Wit M, Dilek Y (2014) Four billion years of ophiolites reveal secular trends in oceanic crust formation. Geosci Front 5:571–603

Gahlan HA (2003) Geology of the area of Wadi Fiqo, South Eastern Desert, Egypt. M.Sc. Thesis, Assiut University, Assiut, Egypt, p 141

Gahlan H (2006) Petrological characteristics of the mantle section in the Proterozoic ophiolites from the Pan African Belt. Ph.D. Thesis, Kanazawa Univ, Japan, p 227

Gahlan H, Arai S (2009) Carbonate-orthopyroxenite lenses from the Neoproterozoic Gerf ophiolite, South Eastern Desert, Egypt: the first record in the Arabian Nubian Shield ophiolites. J Afr Earth Sci 53:70–82

Gahlan H, Arai S, Abu El-Ela F, Tamura A (2012) Origin of Wehrlite Cumulates in the Moho Transition Zone of the Neoproterozoic Ras Salatit Ophiolite, Central Eastern Desert, Egypt: Crustal Wehrlites with Typical Mantle Characteristics. Contrib Mineral Petrol 163 (2):225–241

Gahlan H, Arai S, Almadani S (2015a) Petrogenesis of carbonated meta-ultramafic lenses from the Neoproterozoic Heiani ophiolite, South Eastern Desert, Egypt: a natural analogue to CO_2 sequestration. J Afr Earth Sci 102:102–115

Gahlan H, Azer M, Khalil AES (2015b) The Neoproterozoic Abu Dahr ophiolite, South Eastern Desert, Egypt: petrological characteristics and tectonomagmatic evolution. Mineral Petrol 109:611–630

Gahlan HA, Azer MK, Asimow PD (2018) On the relative timing of listwaenite formation and chromian spinel equilibration in serpentinites. Amer Mineral 103:1087–1102

Gamal El Dien HM, Hamdy MM, Abu El Ela A, Abu Alam T, Hassan A, Kil Y, Mizukami T, Soda Y (2016) Neoproterozoic serpentinites from the Eastern Desert of Egypt: insights into Neoproterozoic mantle geodynamics and processes beneath the Arabian-Nubian Shield. Precam Res 286:213–233

Garson MS, Shalaby IB (1976) Precambrian-Lower Paleozoic plate tectonics and metallogenesis in the Red Sea Region. Spec Pap Geol Assoc Canada 14:573–596

Gass IG (1977) The evolution of the Pan African crystalline basement in NE Africa and Saudi Arabia. J Geol Soc 134:129–138

Gass IG (1981) Pan African (Upper Proterozoic) plate tectonics of the Arabian Nubian Shield. In: Kröner A (ed) Precambrian Plate Tectonics. Elsevier, Amsterdam, pp 387–405

Ghoneim MF (2003) Origin of magnesite veins in serpentinites from Mount El Rubshi and Mount El-Maiyit, Eastern Desert. Egypt Arch Mineral 54:41–63

Ghoneim MF, Salem IA, Hamdy MM (1999) On the petrogenesis of magnesite from Gebel El-Maiyit, Central Eastern Desert. Egypt Fourth International Conference on Geology of the Arab World, Cairo University, Egypt 1:575–593

Ghoneim MF, Salem IA, Hamdy MM (2003) Origin of magnesite veins in serpentinites from Mount El-Rubshi and Mount El-Maiyit, Eastern Desert. Egypt Archi Mineral 54:41–63

González-Jiménez JM, Kerestedjian T, Proenza JA, Gervilla F (2009) Metamorphism on chromite ores from the Dobromirtsi ultramafic Massif, Rhodope Mountains (SE Bulgaria). Geol Acta 7:413–429
Green DH (1961) Ultramafic breccias from the Musa Valley, eastern Papua. Geol Mag 98:1–26
Greenwoods WR, Hadley DJ, Anderson RE, Fleck RJ, Schmidt DL (1976) Late Proterozoic cratonization in southwestern Saudi Arabia. Phil Trans Royal Soc London A280:517–527
Greiling RO (1985) Thrust tectonics in Pan-African rocks of SE Egypt. Terra Cognita 5
Greiling RO (1997) Thrust tectonics in crystalline domains: the origin of a gneiss dome. Proc Ind Acad Sci (Earth Planet Sci) 106:209–220
Gülacar OF, Delaloye M (1976) Geochemistry of nickel, cobalt and copper in Alpine-type ultramafic rocks. Chem Geol 17:269–280
Halls C, Zhao R (1995) Listwaenite and related rocks: perspectives on terminology and mineralogy with reference to an occurrence at Cregganbaun, Co., Mayo. Republic of Ireland Miner Deposita 30:303–313
Hamdy MM, Abu El-Ela AM, Hassan AM, Kil Y, Gamal El Dien HM (2013) Subduction-related cryptic metasomatism in fore-arc to nascent fore-arc Neoproterozoic mantle peridotites beneath the Eastern Desert of Egypt: mineral chemical and geochemical evidences. 15: EGU2013–14056 (abstract)
Hamdy MM, Gamal El Dien HM (2017) Nature of serpentinization and carbonation of ophiolitic peridotites (Eastern Desert, Egypt): constrains from stable isotopes and whole rock geochemistry. Arab J Geosci 10(19):429
Hamdy MM, Lebda EM (2007) Metamorphism of ultramafic rocks at Gebel Arais and Gebel Malo Grim, Eastern Desert, Egypt: mineralogical and O-H stable isotopes constraints. Egypt J Geol 51:105–124
Hamimi Z (1996) Tectonic evolution of the shield rocks of Gabal El Sibai area, Central Eastern Desert. Egypt Egypt J Geol 40:423–453
Hamimi Z, Abd El-Wahed MA, Gahlan HA, Kamh SZ (2019) Tectonics of the Eastern Desert of Egypt: key to understanding the neoproterozoic evolution of the Arabian-Nubian Shield (East African Orogen). In: Bendaoud A et al (eds) The geology of the Arab world—an overview. Springer Geology, Switzerland, pp 1–82
Hamimi Z, Abd El-Wahed MA (2020) Suture(s) and Major Shear Zones in the Neoproterozoic Basement of Egypt. In: Hamimi Z, El-Barkooky A, Martínez Frías J, Fritz H, Abd El-Rahman Y (eds), The geology of Egypt, regional geology reviews, Springer Nature Switzerland, pp 153–189. https://doi.org/10.1007/978-3-030-15265-9_2
Hamimi Z, El-Fakharani A, Emam A, Barreiro JG, Abdelrahman E, Abo-Soliman MY (2018) Reappraisal of the kinematic history of Nugrus shear zone using PALSAR and microstructural data: implications for the tectonic evolution of the Eastern Desert tectonic terrane, northern Nubian Shield. Arab J Geosci 11(17):494
Harraz HZ (2000) A genetic model for a mesothermal Au deposit: evidence from fluid inclusions and stable isotopic studies at El-Sid Gold Mine, Eastern Desert. J Afr Earth Sci 30:267–282
Hassan MA, Hashad AH (1990) Precambrian of Egypt. In: Said R (ed) The geology of Egypt. Balkema, Rotterdam, pp 201–245
Hébert R, Adamson AC, Komor SC (1990) Metamorphic petrology of ODP Leg 109, Hole 670A serpentinized peridotites: serpentinization processes at a slow spreading ridge environment. In: Detrick R, Honnorez J, Bryan WB, Juteau T et al (eds), Proceedings of the Ocean Drilling Program, Scientific Results (106/109, College station, Texas (Ocean Drilling Program), pp 103–115
Hess HH, Smith RJ, Dengo G (1952) Antigorite from the vicinity of Caracas, Venezuela. Amer Mineral 37:68–75
Hume WF (1934) Geology of Egypt. The fundamental Precambrian rocks of Egypt and the Sudan, Part l, The metamorphic rocks, vol 2. Geol Surv Egypt, Cairo, p 300
Hume WF (1937) The geology of Egypt, vol II, Part III. Geological Survey of Egypt, Cairo
Huson R, Kusky TM, Li JH (2004) Geochemical and petrographic characteristics of the central belt of the Archean Dongwanzi ophiolite complex. In: Kusky TM (ed) Precambrian ophiolites and related rocks. Elsevier, Amsterdam, pp 283–320
Hussein AA (1990) Mineral deposits of Egypt. Chapter 26. In: Said R (ed), The geology of Egypt, pp 511–566
Irvine TN (1965) Chromian spinel as petrogenetic indicator, part I. Theory Canadian J Earth Sci 2:648–671
Ishii T, Robinson PT, Maekawa H, Fiske R (1992) Petrological studies of peridotites from diapiric Serpentinite Seamounts in the Izu-Ogasawara-Mariana forearc, leg 125. In: Pearce JA, Stokking LB, et al (Eds), Proceedings of the Ocean Drilling Project, Leg 125, Scientific Results (College Station), pp 445–485
Ishiwatari A, Sokolov SD, Vysotskiy SV (2003) Petrological diversity and origin of ophiolites in Japan and Far East Russia with emphasis on depleted harzburgite. In Dilek Y, Robinson PT (eds.) Ophiolites in Earth History. Geol Soc London Spec Publ 218: 597–617
Ismael IS, Hassan MS (2008) Characterization of some Egyptian serpentinites used as ornamental stones. Chin J Geochem 27 (2):140–149
Jackson ED, Thayer TP (1972) Some criteria for distinguishing between stratiform, concentric and alpine peridotite–gabbro complexes. 24th International Geological Congress 2: 297–302
Jan MQ, Windley BF (1990) Chromian spinel–silicate chemistry in ultramafic rocks of the Jijal complex, northwest Pakistan. J Petrol 31:667–715
Janecky DR, Seyfried WE (1986) Hydrothermal serpentinization of peridotite within the oceanic crust: experimental investigations of mineralogy and major element chemistry. Geochim Cosmochim Acta 50:1357–1378
Jaques AL, Green DH (1980) Anhydrous melting of peridotite at 0–15 kbar pressure and the genesis of tholeiitic basalt. Contrib Mineral Petrol 73:287–310
Johannes W (1969) An experimental investigation of the system MgO–SiO_2–H_2O–CO_2. Amer J Sci 267:1083–1104
Johannes W (1970) Zur Entstehung von Magnesitvorkommen. Neues Jb Miner Abh 113:274–325
Katz O, Beyth M, Miller N, Stern R, Avigad D, Basu A, Anbar A (2004) A Late Neoproterozoic (630 Ma) boninitic suite from southern Israel: implications for the consolidation of Gondwana-land. Earth Planet Sci Lett 218:475–490
Kelemen PB (1990) Reaction between ultramafic rock and fractionating basaltic magma I. Phase relations, the origin of calc-alkaline magma series, and the formation of discordant dunite. J Petrol 31:55–98
Kelemen PB, Shimizu N, Salters VJM (1995) Extraction of mid-ocean-ridge basalt from the upwelling mantle by focused flow of melt in dunite channels. Nature 375:747–753
Khalil AES, Azer MK (2007) Supra-subduction affinity in the Neoproterozoic serpentinites in the Eastern Desert, Egypt: evidence from mineral composition. J Afr Earth Sci 49:136–152
Khalil AES, Obeid MA, Azer MK (2014) Serpentinized peridotites at the north part of Wadi Allaqi district (Egypt): implications for the tectono-magmatic evolution of fore-arc crust. Acta Geol Sin 88 (5):1421–1436
Khalil KI (2007) Chromite mineralization in ultramafic rocks of the Wadi Ghadir area, Eastern Desert, Egypt: mineralogical, micro-chemical and genetic study. Neues Jb Miner Abh 183:283–296

Khalil KI, Helba HA, Mücke A (2003) Genesis of the gold mineralization at the Dungash gold mine area, Eastern Desert, Egypt: A mineralogical-microchemical study. J Afr Earth Sci 37:111–122

Khudeir AA (1983) Geology of the Rubshi ophiolite association, Central Eastern Desert, Egypt. Ph.D. Thesis, Assiut University, Egypt

Khudeir AA (1995) El-Genina El-Gharbia and El-Genina El-Sharkia ultramafic-mafic intrusions, Eastern Desert, Egypt: geology, petrology, geochemistry and petrogenesis. Bull Fac Sci Assiut Univ, 177–219

Klein F, Garrido CJ (2011) Thermodynamic constraints on mineral carbonation of serpentinized peridotite. Lithos 126:147–160

Klemm D, Klemm R (2013) Gold and gold mining in ancient Egypt and Nubia: Berlin, Springer, p 649

Klemm D, Klemm R, Murr A (2001) Gold of the Pharaohs–6000 years of gold mining in Egypt and Nubia. J Afr Earth Sci 33(3–4):643–659

Kröner A, Greiling R, Reischmann T, Hussein IRM, Stern RJ, Dürr S, Krüger J, Zimmer M (1987) Pan-African Crustal evolution in the Nubian segment of Northeast Africa. In Kröner A (ed.), Proterozoic Lithosphere Evolution. Amer Geophys Union Geodyn Ser 17: 235–257

Kröner A, Todt W, Hussein IM, Mansour M, Rashwan AA (1992) Dating of late Proterozoic ophiolites in Egypt and Sudan using the single grain zircon evaporation technique. Precamb Res 59:15–32

Kushiro I (1969) The system forsterite-diopside-silica with and without water at high pressures. Amer J Sci 267A:269–294

Kusky TM (2004) Precambrian ophiolites and related rocks. Elsevier, Amsterdam, p 748

Kusky TM, Abdelsalam M, Tucker R, Stern RJ (2003) Evolution of the East African and related Orogens, and the assembly of Gondwana. Precam Res 123:81–344

Kusky TM, Li JH, Tucker RD (2001) The Archean Dongwanzi ophiolite complex, North China Craton: 2.505-billion-year-old oceanic crust and mantle. Science 292:1142–1145

Kusky TM, Ramadan TM (2002) Structural controls on Neoproterozoic mineralization in the South Eastern Desert, Egypt: an integrated field, Landsat TM, and SIR-C/X SAR approach. J Afr Earth Sci 35:107–121

Lago BL, Rabinowicz M, Nicolas A (1982) Podiform chromite ore bodies: a genetic model. J Petrol 23:103–125

Ledru P, Auge T (1984) The Al Ays ophiolitic complex; petrology and structural evolution. Saudi Arabian Deputy Ministry for Mineral Resources Open-File Report BRGM-OF-04–15

Li JH, Kusky TM, Huang X (2002) Archean podiform chromitites and mantle tectonites in ophiolitic mélange, North China Craton: a record of early oceanic mantle process. Geol Soc Amer Today 12 (7):4–11

Li Z-XA, Lee C-TA (2006) Geochemical investigation of serpentinized oceanic lithospheric mantle in the Feather River Ophiolite, California: implications for the recycling rate of water by subduction. Chem Geol 235:161–185

Liipo J, Vuollo J, Nykänen V, Piirainen T, Pekkarinen L, Tuokko I (1995) Chromites from the early Proterozoic Outokumpu-Jormua ophiolite belt: a comparison with chromites from Mesozoic ophiolites. Lithos 36:15–27

Malpas J (1978) Magma generation in the upper mantle, field evidence from ophiolite suites and application to the generation of oceanic lithosphere. Phil Trans Royal Soc London 288:527–546

Martin B, Fyfe WS (1970) Some experimental and theoretical observations on the kinetics of hydration reactions with particular reference to serpentinization. Chem Geol 6:185–202

Matsumoto I, Arai S (2001) Morphological and chemical variations of chromian spinel in dunite-harzburgite complexes from the Sangun zone (SW Japan): implications for mantle/melt reaction and chromitite formation processes. Mineral Petrol 73:305–323

Mellini M, Rumori C, Viti C (2005) Hydrothermally reset magmatic spinels in retrograde serpentinites: formation of "ferritchromit" rims and chlorite aureoles. Contrib Mineral Petrol 149:266–275

Mercier J-C, Nicolas A (1975) Textures and fabrics of upper-mantle peridotites as illustrated by xenoliths from basalts. J Petrol 16 (2):454–487

Mével C (2003) Serpentinization of abyssal peridotite at mid-ocean-ridges. Comptes Rendus Geosciences 335:825–852

Moores EM, Vine FJ (1971) The Troodos Massif, Cyprus and other Ophiolites as oceanic crust; evaluation and implications. Phil Trans Royal Soc London A268:433–466

Murton B (1989) Tectonic controls on boninite genesis. Geological Society, London, Special Publications 42(1):347–377

Mysen BO, Kushiro I (1977) Compositional variations of coexisting phases with degree of melting of peridotite in the upper mantle. Amer Mineral 62:843–865

Nasr BB, Beniamin NY, Sadek MF, Abd Elmigid E, Smith M (1996) The Geological and tectonic study of the Gerf ultrabasic complex, south Eastern Desert, Egypt. Proc Geol Surv Egypt Cenn Conference, 635–643

Nasr BB, Beniamin NY (2001) Ophiolite sequence of Gerf-Hasium and Sol Hamed-Shiab areas, South Eastern Desert, Egypt. Ann Geol Surv Egypt XXIV:63–78

Nassief MO, Macdonald R, Gass IG (1984) The Jebel Thurwah upper Proterozoic ophiolite complex, western Saudi Arabia. Geol Soc London 141:537–546

Neary CR, Gass IG, Cavanagh BJ (1976) Granitic association of northwestern Sudan. Geol Soc Amer Bull 87:1501–1512

Nozaka T (2003) Compositional heterogeneity of olivine in thermally metamorphosed serpentinite from Southwest Japan. Amer Mineral 88:1377–1384

O'Hanley DS (1996) Serpentinites. Oxford University Press, Oxford, p 277

Obeid MA, Khalil AES, Azer MK (2016) Mineralogy, geochemistry and geotectonic significance of the Neoproterozoic ophiolite of Wadi Arais area, south Eastern Desert. Egypt Inter Geol Rev 58:687–702

Ohara Y, Ishii T (1998) Peridotites from southern Marian forearc: heterogeneous fluids supply in mantle wedge. Island Arc 7:541–558

Ohara Y, Stern RJ, Ishii T, Yurimoto H, Yamazaki T (2002) Peridotites from the Mariana Trough: first look at the mantle beneath an active back-arc basin. Contrib Mineral Petrol 143(1):1–18

Page NJ (1967) Serpentinization at Burro Mountain, California. Contrib Mineral Petrol 14:321–342

Paktunc AD (1990) Origin of podiform chromite deposits by multistage melting, melt segregation and magma mixing in upper mantle. Ore Geol Rev 5:211–222

Pallister JS, Stacy JS, Fischer LB, Premo WR (1989) Precambrian ophiolites of Arabia: geologic setting U-Pb geochronology, Pb-isotope characteristics, and implication for continental accretion. Precam Res 38:1–54

Parkinson IJ, Pearce JA (1998) Peridotites from the Izu–Bonin–Mariana forearc (ODP Leg 125): evidence for mantle melting and melt–mantle interaction in a supra-subduction zone setting. J Petrol 39(9):1577–1618

Pearce JA (2003) Subduction zone ophiolites. In: Dilek Y, Newcomb S (eds), Ophiolite concept and the evolution of geological thought. Geol Soc Am Spec Pap 373:269–294

Pearce JA, Barker P, Edwards S, Parkinson I, Leat P (2000) Geochemistry and tectonic significance of peridotites from the South Sandwich arc–basin system. South Atlantic Contrib Mineral Petrol 139(1):36–53

Pearce JA, Lippard SJ, Roberts S (1984) Characteristics and tectonic significance of supra-subduction zone ophiolites. In Kokelaar BP, Howells MF (eds), Marginal Basin Geology. Geol Soc London Spec Publ 16:77–94

Peltonen P, Kontinen A (2004) The Jormua ophiolite: A mafic–ultramafic complex from an ancient Ocean-Continent Transition Zone. In: Kusky TM (ed) Precambrian ophiolites and related rocks. Elsevier, Amsterdam, pp 35–72

Pereira MD, Shaw DM, Acosta A (2003) Mobile trace elements and fluid-dominated processes in the Ronda peridotites, South Spain. Canad Mineral 41:617–625

Pfänder JA, Kröner A (2004) Tectono–magmatic evolution, age and emplacement of the Agardagh Tes-Chem ophiolite in Tuva, Central Asia: crustal growth by island arc accretion. In: Kusky TM (ed) Precambrian ophiolites and related rocks. Elsevier, Amsterdam, pp 207–222

Quick JE (1981) The origin and significance of large, tabular dunite bodies in the Trinity peridotite, northern California. Contrib Mineral Petrol 78:413–422

Quick JE (1990) Geology and origin of late Proterozoic Darb Zubaydah ophiolite, Kingdom of Saudi Arabia. Geol Soc Amer Bull 102:1007–1020

Rittmann A (1958) Geosynclinal volcanism, ophiolites and Barramiya rocks. Egypt J Geol 2:61–66

Roberts S (1992) Influence of partial melting regime on the formation of ophiolitic chromite. In Parson LM, Murton BJ, Browning P (eds), Ophiolites and their Modern Oceanic Analogues. Geol Soc Spec Publ 60:203–217

Saleh GM (2006) The chromite deposits associated with ophiolite complexes, southeastern Desert, Egypt: Petrological and geochemical characteristics and mineralization. Chin J Geochem 25(4):307–317

Salem IA, Ghoneim MF, Zahran AA, Hamdy MM (1997) Petrology and genesis of the ultramafic-hosted vein magnesite deposits at G. El-Rubshi, central Eastern Desert, Egypt. Conference on Geochemistry, 3rd (Alexandria, 1997), Proc. Alexandria, Alexandria University: 241–267

Salters VJM, Stracke A (2004) Composition of the depleted mantle. Geo-chem Geophys Geosys 5:Q05B07

Scott DJ, Helmstaedt H, Bickle MJ (1992) Purtuniq ophiolite, Cape Smith Belt, northern Quebec, Canada: a reconstructed section of early Proterozoic oceanic crust. Geology 20:173–176

Seyfried WEJ, Dibble WE (1980) Seawater–peridotite interaction at 300 °C and 500 bars: implications for the origin of oceanic serpentinites. Geochim Cosmochim Acta 44:309–321

Shackleton RM (1994) Review of late Proterozoic sutures, ophiolitic mélanges and tectonics of eastern Egypt and northeastern Sudan. Geol Rundsch 83:537–546

Shackleton RM, Ries AC, Graham RH, Fitches WR (1980) Late Precambrian ophiolitic mélange in the Eastern Desert of Egypt. Nature 285:472–474

Shervais JW, Kimbrough DL, Renne PR, Hanan BB, Murchey B, Snow CA, Schuman MMZ, Beaman J (2004) Multi-stage origin of the Coast Range Ophiolite. California; Implications for the life cycle of supra-subduction zone ophiolites. Inter Geol Rev 46:289–315

Shiga Y (1983) Origin of nickel and cobalt in ore deposits of the Kamaishi mining district, northeastern Japan. Mining Geol 33:385–398 (in Japanese with English abstract)

Shiga Y (1987) Behavior of iron, nickel, cobalt and sulfur during serpentinization, with reference to the Hayachine ultramafic rocks of the Kamaishi mining district, northeastern Japan. Canad Mineral 25:611–624

Sinton JM (1977) Equilibration history of the basal alpine-type peridotite, Red Mountain, New Zealand. J Petrol 18:216–246

Snow JE, Dick HJB (1995) Pervasive magnesium loss by marine weathering of peridotite. Geochim Cosmochim Acta 59:4219–4235

Sobolev NV, Logvinova AM (2005) Significance of accessory chrome spinels in identifying serpentinite paragenesis. Inter Geol Rev 47:58–64

Stein M, Goldstein SL (1996) From plume head to continental lithosphere in the Arabian Nubian Shield. Nature 382:773–778

Stern RJ (1994) Arc assembly and continental collision in the Neoproterozoic East African Orogen: implications for the assembly of Gondwanaland. Ann Rev Earth Planet Sci 22:319–351

Stern RJ (2004) Subduction initiation: spontaneous and induced. Earth Planet Sci Lett 226:275–292

Stern RJ, Johnson PR, Kröner A, Yibas B (2004) Neoproterozoic ophiolites of the Arabian-Nubian Shield. In: Kusky TM (ed), Precambrian Ophiolites and Related Rocks. In: Developments in Precambrian Geology 13:95–128

Stern RJ, Kroner A, Manton WI, Reischmann T, Mansour M, Hussein IM (1989) Geochronology of the late Precambrian Hamisana shear zone, Red Sea Hills, Sudan and Egypt. J Geol Soc London 146:1017–1030

Stern RJ, Nielsen KC, Best E, Sultan M, Arvidson RE, Kröner A (1990) Orientation of late Precambrian sutures in the Arabian-Nubian shield. Geology 18:1103–1106

Streckeisen A (1976) To each plutonic rock its proper name. Earth-Science Reviews 12(1):1–33

St-Onge MR, Lucas SB, Scott DJ, Begin NJ (1989) Evidence for the development of the oceanic crust and for continental rifting in tectonostratigraphy of the early Proterozoic Cape Smith belt. Geosciences Canada 16:119–122

Suita MTF, Strieder AJ (1996) Cr-spinel from Brazilian mafic-ultramafic complexes: metamorphic modifications. Int Geol Rev 38:245–267

Surour AA (2019) Mid-ocean ridge vs. forearc and subduction settings: clues from rodingitization of tectonic fragments in the Neoproterozoic ophiolites of the Eastern Desert. Egypt. Lithos 342:18–30

Takahashi E, Kushiro I (1983) Melting of a dry peridotite at high pressures and basalt magma genesis. Amer Mineral 68:859–879

Takla MA, Basta FF, Surour AA (1992) Petrology and mineral chemistry of rodingites associating the pan-African ultramafics of Sikait-Abu Rusheid area, south Eastern Desert. Egypt Geology of the Arab World 1:491–507

Takla MA, Noweir AM (1980) Mineralogy and mineral chemistry of ultramafic mass of El-Rubshi, Eastern Desert. Egypt Neues Jb Miner Abh 140:17–28

Takla MA, Noweir AM, Ali SA (1975) Ore mineralogy of the serpentinites of Bir El-Kubbaniya Um Khors area. Egypt Chem Erde 34:244–250

Takla MA, Surour AA (1996) On the occurrence of Ni sulphides and arsenides in some Egyptian serpentinites. Egypt Minerals 8:1–18

Tamura A, Makita M, Arai S (1999) Petrogenesis of ultramafic rocks in the Kamuikotan belt, Hokkaido, northern Japan. Mem Geol Soc Japan 52:53–68 (in Japanese with English abstract)

Teklay M (2006) Neoproterozoic arc-back-arc system analog to modern arc-back-arc systems: evidence from tholeiite-boninite association, serpentinite mudflows and across-arc geochemical trends in Eritrea, southern Arabian-Nubian shield. Precam Res 145:81–92

Thayer TP (1964) Principle features and origin of podiform chromite deposits and some observations on the Guleman-Soridag district, Turkey. Econ Geol 59:1497–1542

Vuollo J, Liipo J, Nykänen V, Piirainen T, Pekkarinen L, Tuokko I, Ekdahl E (1995) An early Proterozoic podiform chromitite in the Outokumpu ophiolite complex, Finland. Econ Geol 90:445–452

Whittaker EJW, Zussman J (1956) The characterization of serpentine minerals by X-ray diffraction. Mineral Mag 31:107–126

Wicks FJ, Whittaker EJW (1977) Serpentine textures and serpentinization. Canad Mineral 15:459–488

Winter JD (2001) An introduction to igneous and metamorphic petrology. Prentice Hall, p 697

Wolde B, Asres Z, Desta Z, Gonzalez JJ (1993) Neoproterozoic zirconium-depleted boninite and tholeiitic series rocks from Adola, southern Ethiopia. Precam Res 80:261–279

Wynne-Edwards HR (1976) Proterozoic ensialic orogenesis: the millipede model of ductile plate tectonics. Amer J Sci 276:927–953

Yibas B, Reimold WU, Anhaeusser CR, Koeberl C (2003) Geochemistry of the mafic rocks of the ophiolitic fold and thrust belts of southern Ethiopia: constraints on the tectonic regime during the Neoproterozoic (900–700 Ma). Precam Res 121:157–183

Zhou M-F, Robinson PT, Bai W-J (1994) Formation of podiform chromitites by melt/rock interaction in the upper mantle. Miner Depos 29:98–101

Zhou M-F, Robinson PT, Malpas J, Li Z (1996) Podiform chromitites in the Luobusa ophiolite (southern Tibet): implications for melt-rock interaction and chromite segregation in upper mantle. J Petrol 37:3–21

Zimmer M, Kröner A, Jochum KP, Reischmann T, Todt W (1995) The Gabal Gerf complex: a Precambrian N-MORB ophiolite in the Nubian Shield, NE Africa. Chem Geol 123:29–51

Zoheir B, Lehmann B (2011) Listvenite-lode association at Barramiya gold mine, Eastern Desert. Egypt Ore Geol Rev 39:101–115

Zoheir B, Moritz R (2014) Fluid evolution in the El-Sid gold deposit, Eastern Desert, Egypt. In: Garofalo PS, Ridley JR (eds), Gold-transporting hydrothermal fluids in the Earth's crust. Geol Soc Spec Publ London, p 402